Three-phase boundary lines of some random media

Dominique Jeulin

Three-phase boundary lines of some random media

Dominique Jeulin
Mines Paris, PSL University
Centre des Matériaux P. M. Fourt, Mines Paris
Centre de Morphologie Mathématique, Mines Paris

September 2025

Abstract

Multi components materials show triple phase boundary (TPB) lines at the interface between three components. TPB lines are of primary importance for the performance of electrochemical devices like Solid Oxide Fuel Cells (SOFC). We derive theoretical estimates of the specific length of (TPB) lines $L_{V_{ijk}}$ for a broad range of multi-component random structures. Since analytical results are obtained, random microstructures with optimal $L_{V_{ijk}}$ can be designed. The effects of the composition, through volume fractions, and of the morphology, through the choice of primary grains, are separate, so that "optimal composition" is derived independently on the geometry. $L_{V_{ijk}}$ is inversely proportional to the square of a length scale of the microstructure. Our theoretical approach is validated by comparison of the predicted $L_{V_{ijk}}$ to some published measurements made on 3D images of materials. Various models designed with the same basic ingredients may show a large range of values for $L_{V_{ijk}}$, depending on their mode of construction. Much longer $L_{V_{ijk}}$ than experimental measurements in real materials can theoretically be reached, typically over an order of magnitude. This can be used as a guideline to improve the electrochemical behavior of fuel cell components.

Contents

1 Introduction **3**

2 Estimation of the mean length of the triple boundary lines **4**

3 Previous analytical prediction models of TPB lines **5**

4 Multi-component mosaic model **6**
4.1 Voronoï mosaic 10
4.2 Delaunay mosaic 11
4.3 Poisson and STIT mosaics 12
4.4 Dead Leaves mosaic 13

5 Multi-components Color Dead Leaves **16**

6 Three components models based on the superposition of independent random sets **25**
6.1 Superposition of Boolean models 28
6.2 Superposition of two-components mosaics 30
6.3 Superposition of Color Dead Leaves models 31
6.4 Superposition of random sets generated by dilution random functions 33
6.4.1 Random set A_1 35
6.4.2 Random set A_2 36
6.4.3 Random set A_3 38
6.4.4 Random set A_4 40
6.4.5 Random set A_n 41
6.5 Superposition of excursion random sets of dilution random functions 42
6.5.1 Random set $A_N(2)$ 43
6.5.2 Random set $A_N(3)$ 44
6.5.3 Random set $A_N(4)$ 45
6.5.4 Random set $A_N(m)$ 46
6.6 Superposition of random sets generated by two thresholds of dilution random functions 47
6.7 Superposition of truncated Gaussian random functions 49
6.8 Superposition of random sets defined by two thresholds of independent Gaussian RF 52

7 Discussion **55**
7.1 Potential Texture Optimization with respect to TPB lines . . 56
7.2 Predictive ability of the models 56
7.3 3D versus 2D information for TPB lines 58

8 Conclusion **58**

1 Introduction

In $\mathbb{R}^3$ multi-component random sets with more than two components show triple phase boundary (TPB) lines at the intersection of three components. These lines at the intersection of pores and of two solid components of devices like Solid Oxide Fuel Cells (SOFC) are of primary importance for their performance: electrochemical reactions develop in the zone of intersection of the electron conducting component, the oxygen-ion conducting component, and the pores for the transport of H_2 and H_20. An illustration of TPB lines extracted from a 3D micromographic image is shown on Figure 1 [11].

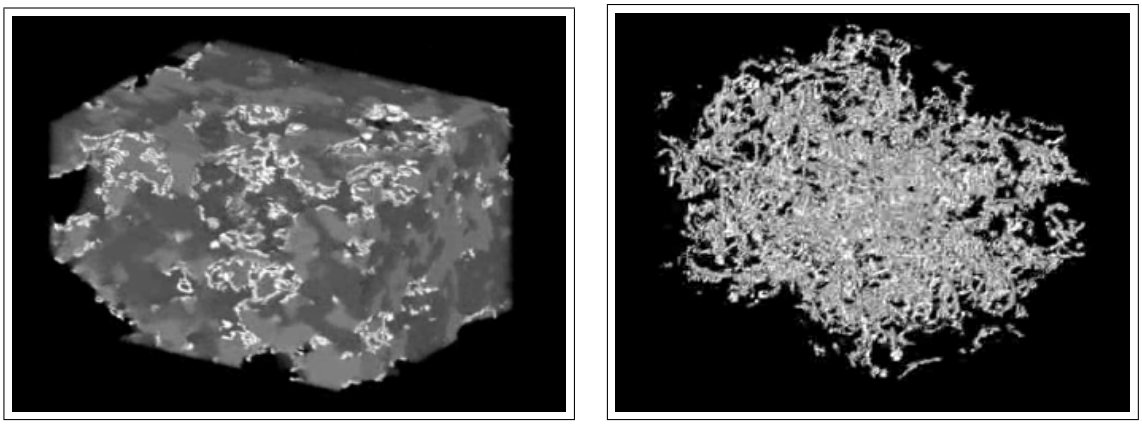

Figure 1: TPB lines in a three-components SOFC material [11]

To measure in materials the length per unit volume of TPB lines between components i, j, k, L_{Vijk}, some studies were made from 3D microstructure reconstructions by FIB-SEM serial sections, or by X-ray microtomography [20], [21], [19], [18], [15].

In another context, triple lines occur at the interface with three different types of crystals (for instance defined by their orientation) in polycrystals. Our methodology can be applied as well in this context.

In what follows, we compute theoretical estimates of the mean length of the triple boundary lines per unit volume L_{Vijk} of some models of random

media [8] that can be of interest for applications. The results enable us to compare various types of microstructures from the point of view of L_{Vijk}. We show that a wide range of values of L_{Vijk} can be obtained on microstructures with similar ingredients, even far beyond the values observed in presently available real materials, opening the way towards improved physical properties.

After a reminder of existing random models predicting L_{Vijk}, we introduce a way to estimate L_{Vijk} from third order morphological moments. It is then applied to various types of morphological models of multi-component random media, for which detailed calculations are provided: mosaic model, Color Dead Leaves, and 3 components models generated by the superposition of independent random sets, applied to the Boolean model, the Dead Leaves model, the Dilution model, and to truncated Gaussian random functions. Finally, a comparison of the performances of different types of random models is discussed, and some predictions of L_{Vijk} are compared to available measurements made on materials.

2 Estimation of the mean length of the triple boundary lines

Any random curve with locally finite length in $\mathbb{R}^3$ intersects a reference plane with points. If N_A is the average number of points of intersection per unit area, the length of the curve per unit volume L_V, namely specific length, for stationary isotropic random curves is estimated by the expression [2]:

$$L_V = 2N_A \tag{1}$$

From equation (1), it comes out that L_V for a 3D structure can be estimated with planar observations. No information in 3D is required. In the case of anisotropic structures, measurements in several planar observations with various orientations have to be averaged.

Consider now a multi-component random set with m components A_1, A_2, ..., A_m with $m \geq 3$). For any pair A_i, A_j we have $A_i \cap A_j = \emptyset$. The specific area of contact between A_i and A_j, S_{Vij} can be estimated from the cross-covariance $C_{ij}(h) = P(x \in A_i,\ x + h \in A_j)$. In the isotropic case, $S_{Vij} = 4C'_{ij}(0)$. For any triple A_i, A_j, A_k the specific length of the line of contact between A_i, A_j, and A_k, L_{Vijk} is estimated from the second order derivatives of third order moments $P_{ijk}(h_1, h_2) = P(x \in A_i,\ x + h_1 \in A_j,\ x + h_2 \in A_k)$. To show this point, we consider the estimation of the specific number of triple points per unit area by the probability $P_{ijk}(h_1, h_2)$ for $h_1 \rightarrow$

$0, h_2 \to 0$. Using a second order Taylor expansion of $P_{ijk}(h_1, h_2)/(h_1 h_2)$ around $h_1 = 0, h_2 = 0$, we get for the specific number of triple points $N_{A_{ijk}}$:

$$N_{A_{ijk}} = \lim_{h_1 \to 0, h_2 \to 0} P_{ijk}(h_1, h_2)/(h_1 h_2) = \left(\frac{\partial^2 P_{ijk}(h_1, h_2)}{\partial h_1 \partial h_2} \right)_{h_1=0, h_2=0}$$

Therefore, in the isotropic case, for any pair of orthogonal vectors $\{h_1, h_2\}$ it comes for the estimator of the mean length of triple boundary lines L^*_{Vijk}:

$$L^*_{Vijk} = 2 \sum_{i,j \neq i,k \neq i,j} \left(\frac{\partial^2 P_{ijk}(h_1, h_2)}{\partial h_1 \partial h_2} \right)_{h_1=0, h_2=0} \tag{2}$$

In what follows we will mainly consider the case of three components ($m = 3$), and will provide estimates of L_{Vijk} based on equation (2). In order to consider all configurations of triplet $\{i, j, k\}$, we will have to explore the results obtained by the six permutations of the triplet and to estimate L_{Vijk} by summing the results obtained for each permutation. For each configuration $\{i, j, k\}$, triple points are extracted by four rotations of orthogonal vectors $\{h_1, h_2\}$ in the plane and L^*_{Vijk} in equation (2) has to be averaged over these rotations. In the isotropic case, each rotation of the pair $\{h_1, h_2\}$ provides the same result, so that we can restrict the extraction of triple points to the six configurations for $\{i, j, k\}$. When dealing with more than three components ($m > 3$)), $m(m-1)(m-2)$ configurations have to be considered to estimate the total number of triple points over all components.

We have to point out that the use of configurations to estimate L^*_{Vijk} by equation ((2) is prone to biases, depending on the model of microstructure. This is detailed for the estimation of the connectivity number in 2D in the case of the Boolean model in ([8], p. 214). The bias introduced by equation ((2) is estimated in section 6 by comparison to the prediction of unbiased estimates, and therefore a correction factor of $\frac{\pi}{2}$ to equation (2) has to be introduced, which becomes:

$$L^*_{Vijk} = \pi \sum_{i,j \neq i,k \neq i,j} \left(\frac{\partial^2 P_{ijk}(h_1, h_2)}{\partial h_1 \partial h_2} \right)_{h_1=0, h_2=0} \tag{3}$$

3 Previous analytical prediction models of TPB lines

As far as we know, very few developments are presently available to predict the length of TPB line from a model of random structure.

The first one is based on random sphere packings ([23], among others). It predicts L_{Vijk} as a function of the coordination numbers between particles of pairs of components, and the particle contact angle. It was used in [21].

A more realistic model according to the real morphology of microstructures encountered in SOFC was proposed in [4], [22], and called "extended microstructure model". Mimicking the growth of crystals from Poisson germs as for the construction of the Voronoï tessellation, it generates a three-component model, A_1, A_2, A_3 with volume fractions P_1, P_2 and P_3. The growth being stopped at a finite time, the union $A_1 \cup A_2 = A_3^c$ builds a Boolean model with pores A_3. Poisson germs with two colors are the seeds of the growth process with two different growth rates. When the isotropic growth is stopped, A_1 and A_2 are made of spheres with radius R_1 and R_2, volumes V_1, V_2 and surface areas S_1, S_2. The growth of two grains with different colors A_1', A_2' stops when they start to overlap, generating a planar interface between A_1 and A_2. A version of the model is based on a non isotropic growth, using non spherical convex particles, like for instance parallelepipeds.

For this model, L_{Vijk} is estimated from classical stereological relationships, providing the expression, given here with our notations:

$$L_{Vijk} = \frac{\pi}{4} \frac{P_1 P_2}{P_1 + P_2} P_3 \left(\log P_3\right)^2 \frac{S_1}{V_1} \frac{S_2}{V_2} \tag{4}$$

A qualitative comparison of the length of TPB lines given by equation (4) and obtained for other models of random media is provided in subsection 7.1.

More recently, an expression of L_{Vijk} was derived in the case of truncated Gaussian random functions [17], for the model developed in [1]. We will come back later to this expression.

4 Multi-component mosaic model

The mosaic model (chapter 8 in [8]) starts from a random tessellation of space into cells C_k. To each cell is assigned a single set A_i with probability P_i, and independently for two separate cells. The m components present some symmetry, and have similar probabilistic properties, up to volume fraction P_i. It is easy to compute the covariance $C_{ii}(h)$ of each component and the cross covariances $C_{ij}(h)$ between A_i and A_j. They are given as a function of the average geometric covariogram of the cell, from

$$r(h) = \frac{\overline{V}(C \cap C_{-h})}{\overline{V}(C)}$$

$\overline{V}$ being the average volume over the realizations of the random cell C. We have ([8], p. 271):

$$C_{ii}(h) = P_i r(h) + P_i^2(1 - r(h))$$

$$C_{ij}(h) = P_i P_j(1 - r(h)$$

The specific surface areas S_{V_i} and specific surface areas of contact S_{Vij} are given as a function of the average surface area $\overline{S}(C)$ of the random cell C, by:

$$S_{V_i} = P_i(1 - P_i)\frac{\overline{S}(C)}{\overline{V}(C)} \tag{5}$$

$$S_{Vij} = P_i P_j \frac{\overline{S}(C)}{\overline{V}(C)}$$

For the third order moment $P_{ijk}(h_1, h_2)$ we need to know the probability $P_3(h_1, h_2)$ that points x, $x + h_1$ and $x + h_2$ belong to three different cells C_i. Following ([8], p. 263), this probability is given by

$$P_3(h_1, h_2) = 1 - P_1(h_1, h_2) - P_2(h_1, h_2)$$

where $P_1(h_1, h_2)$ is the probability that points x, $x + h_1$ and $x + h_2$ belong to a single cell, and $P_2(h_1, h_2)$ is the probability that points x, $x + h_1$ and $x + h_2$ belong to two different cells. Noting $h_3 = h_2 - h_1$, we have

$$P_1(h_1, h_2) = s(h_1, h_2) = \frac{\overline{V}(C \cap C_{-h_1} \cap C_{-h_2})}{\overline{V}(C)}$$

$$P_2(h_1, h_2) = r(h_1) + r(h_2) + r(h_3) - 3s(h_1, h_2)$$

For any number of components $m \geq 3$, $P_{ijk}(h_1, h_2)$ follows from $P_3(h_1, h_2)$ and from the independent affectation of cells to components A_i:

$$P_{ijk}(h_1, h_2) = P_i P_j P_k(1 - r(h_1) - r(h_2) - r(h_3) + 2s(h_1, h_2)) \tag{6}$$

Using Equation (3), it comes for the mosaic model

$$L^*_{Vijk} = 6\pi P_i P_j P_k \left(2 \left(\frac{\partial^2 s(h_1, h_2)}{\partial h_1 \partial h_2} \right)_{h_1=0, h_2=0} - \left(\frac{\partial^2 r(h_3)}{\partial h_1 \partial h_2} \right)_{h_1=0, h_2=0} \right) \tag{7}$$

For any convex set C,$-\overline{V}(C)r\prime(0)$ is equal to the average projected area of C in the direction h and $\overline{V}(C) \left(\frac{\partial^2 s(h_1, h_2)}{\partial h_1 \partial h_2} \right)_{h_1=0, h_2=0}$ is equal to the width of C in the direction h_2. Averaging over orientations, or in the isotropic case,

this second order derivative is proportional to the average width $\overline{b}$ of the random cell C and

$$\left(\frac{\partial^2 s(h_1,h_2)}{\partial h_1 \partial h_2}\right)_{h_1=0,h_2=0} = \frac{\overline{b}}{\overline{\overline{V}}(C)}$$

We have

$$\frac{\partial}{\partial h_1} r(h_3) = \frac{\partial}{\partial h_3} r(h_3)$$

and

$$\begin{aligned} \frac{\partial^2 r(h_3)}{\partial h_1 \partial h_2} &= \frac{\partial^2 r(h_3)}{\partial^2 h_3} \\ \left(\frac{\partial^2 r(h_3)}{\partial h_1 \partial h_2}\right)_{h_1=0,h_2=0} &= r''(0) \end{aligned}$$

and finally, equation (7) becomes using the six configurations of the triplet $\{i,j,k\}$

$$L^*_{Vijk} = 6\pi P_i P_j P_k \left(2\frac{\overline{b}}{\overline{\overline{V}}(C)} - r''(0)\right) \tag{8}$$

For a given random tessellation, and therefore a given random cell C, the mean length L_{Vijk} depends only of the volume fractions P_i, P_j, P_k. In the case of a three components mosaic, we have $P_1 + P_2 + P_3 = 1$. In these conditions, it is easy to show, that the maximum of the product $P_1P_2P_3$ is obtained when $P_1 = P_2 = P_3 = 1/3$. We have

$$\begin{aligned} P_1P_2P_3 &= P_1P_2(1 - P_1 - P_2) \\ \frac{\partial}{\partial P_1} P_1P_2P_3 &= P_2(1 - P_1 - P_2) - P_1P_2 = P_2(1 - 2P_1 - P_2) \\ \frac{\partial}{\partial P_2} P_1P_2P_3 &= P_1(1 - P_1 - 2P_2) \end{aligned}$$

$$\begin{aligned} \frac{\partial}{\partial P_1} P_1P_2P_3 &= 0 \text{ for } 1 - 2P_1 - P_2 = 0 \\ \frac{\partial}{\partial P_2} P_1P_2P_3 &= 0 \text{ for } 1 - P_1 - 2P_2 = 0 \end{aligned}$$

It comes

$$\begin{aligned} P_1 &= 1 - 2P_2 \\ P_2 + 2 - 4P_2 &= 1 \\ P_2 &= 1/3,\ P_1 = 1/3,\ P_3 = 1/3 \end{aligned}$$

For this equirepartition of the components A_1, A_2, A_3 the length L_{V123} is maximized. Examples are provided below. For some of them (Voronoï, Delaunay, Poisson and STIT mosaics given below), the triple lines are made of chains of segment, since they are obtained by partial intersections of hyperplanes.

More generally, for any $m > 3$, the product $P_i P_j P_k$ of any triplet $\{i, j, k\}$ is maximized when $P_i = P_j = P_k = ... = P_m = 1/m$.

Another way to estimate L^*_{Vijk} from planar images, without needs for identification of the underlying random tessellation, is obtained from 2D estimation of the connectivity number $N_A(A_i)$ of component A_i. An estimate of the connectivity number is provided by ([8], p. 108):

$$N^*_A(A_i) = \left(\frac{\partial^2 P_{iii}(h_1, h_2)}{\partial h_1 \partial h_2} \right)_{h_1=0, h_2=0}$$

with ([8], p. 268)

$$P_{iii}(h_1, h_2) = s(h_1, h_2) \left(P_i + 2P_i^3 - 3P_i^2 \right) + (r(h_1) + r(h_2) + r(h_3)) \left(P_i^2 - P_i^3 \right) + P_i^3$$

and therefore

$$N^*_A(A_i) = \left(P_i + 2P_i^3 - 3P_i^2 \right) \frac{\overline{b}}{\overline{V}(C)} + (P_i^2 - P_i^3) r''(0) + P_i^3 \qquad (9)$$

The covariance of component A_i is given by ([8], p. 268):

$$C_{ii}(h) = P_i r(h) + P_i^2 (1 - r(h))$$

from which

$$C''_{ii}(0) = P_i (1 - P_i) r''(0)$$

The derivative $r''(0)$ can be obtained from $C''_{ii}(0)$ and then introduced in equation (9), in order to estimate $\frac{\overline{b}}{\overline{V}(C)}$ from the experimental value of $N^*_A(A_i)$ measured by image analysis ([8], p. 54). Then L^*_{Vijk} is estimated after introduction of $\frac{\overline{b}}{\overline{V}(C)}$ and of $r''(0)$ into equation (8). However, one should be aware of numerical errors in the computation of $r''(0)$ from $C_{ii}(h)$ without resorting to a numerical model, and therefore proceeding to identification of the underlying random tessellation.

Alternatively, on can measure $N^*_A(A_i)$ for at least two components A_i, A_j with quite different volume fractions P_i, P_j. If necessary, two components with similar volume fractions can be merged to form a random set on which N^*_A can be estimated. Since equation (9) is strongly non linear in P_i, systems of linear independent equations are then used to estimate $\frac{\overline{b}}{\overline{V}(C)}$ and $r''(0)$.

4.1 Voronoï mosaic

The Voronoï mosaic is built from a Voronoï tessellation [2]. Starting from a Poisson point process $\{x_k\}$ with intensity θ, cells C_k of the Voronoï tessellation are built as the zones of influence of the points $\{x_k\}$. For this model, $\overline{V}(C) = 1/\theta$ and ([2], p. 380):

$$\begin{aligned} \bar{b} &= \frac{1}{5}\left(\frac{16\pi^5}{243}\right)^{1/3}\Gamma(\frac{1}{3})\theta^{-1/3} \simeq 1.458\theta^{-1/3} \\ \frac{\bar{b}}{\overline{V}(C)} &\simeq 1.458\theta^{-2/3} \end{aligned}$$

For a stationary Voronoï tessellation in $\mathbb{R}^d$, we have ([3], [8], p. 238):

$$P(K) = \theta \int_{\mathbb{R}^d} \exp\left(-\theta\mu_d(F(K,y))\right) dy$$

with

$$F(K,y) = \cup_{x\in K} B(x, d(x,y))$$

Consider for K a pair of points $\{O, l\}$ with length l. When $l = 0$, $F(O,y) = B(O, d(O,y))$. From now on, we operate in $\mathbb{R}^3$, so that $\mu_3 = V$. We have

$$P(l) = \theta \int_{\mathbb{R}^3} \exp\left(-\theta V(F(l,y))\right) dy$$

By derivation with respect to l,

$$P'(l) = -\theta^2 \int_{\mathbb{R}^3} \frac{\partial}{\partial l}\left(V(F(l,y))\right) \exp\left(-\theta V(F(l,y))\right) dy$$

and

$$\begin{aligned} P''(l) &= \theta^3 \int_{\mathbb{R}^3} \left(\frac{\partial}{\partial l}\left(V(F(l,y))\right)\right)^2 \exp\left(-\theta V(F(l,y))\right) dy \\ &\quad -\theta^2 \int_{\mathbb{R}^3} \frac{\partial^2}{\partial l^2}\left(V(F(l,y))\right) \exp\left(-\theta V(F(l,y))\right) dy \end{aligned}$$

We are looking for the derivative $P''(0)$. Since for any sphere, the second derivative $K''(0) = 0$, we have

$$\left(\frac{\partial^2}{\partial l^2}\left(V(F(l,y))\right)\right)_{l=0} = 0$$

and

$$\begin{aligned} P^{''}(0) &= \theta^3 \int_{\mathbb{R}^3} \left(\pi r^2\right)^2 \exp\left(-\theta \frac{4}{3}\pi r^3\right) dv = \theta^3 \int_0^\infty (\pi r^2)^2 \exp\left(-\theta v\right) dv \\ &= \theta^3 \int_0^\infty \pi^2 (\frac{3}{4\pi} v)^{4/3} \exp\left(-\theta v\right) dv \\ &= \theta^3 \pi^2 (\frac{3}{4\pi})^{4/3} \int_0^\infty v^{4/3} \exp\left(-\theta v\right) dv = \theta^2 \theta^{-4/3} \pi^2 (\frac{3}{4\pi})^{4/3} \int_0^\infty v^{4/3} \exp\left(-v\right) dv \end{aligned}$$

$$\int_0^\infty v^{4/3} \exp\left(-v\right) dv = \frac{8}{27}\sqrt{3}\frac{\pi}{\Gamma\left(\frac{2}{3}\right)}$$

and

$$P^{''}(0) = \theta^{2/3} \pi^2 (\frac{3}{4\pi})^{4/3} \frac{8}{27}\sqrt{3}\frac{\pi}{\Gamma\left(\frac{2}{3}\right)}$$

$$\pi^2 (\frac{3}{4\pi})^{4/3} \frac{8}{27}\sqrt{3}\frac{\pi}{\Gamma\left(\frac{2}{3}\right)} = 1.740\,3$$

and

$$P^{''}(0) = 1.740\,3\theta^{2/3}$$

$$r''(0) = \theta^{2/3} \pi^2 (\frac{3}{4\pi})^{4/3} \frac{8}{27}\sqrt{3}\frac{\pi}{\Gamma\left(\frac{2}{3}\right)} \simeq 1.740\,3\theta^{2/3}$$

so that

$$\begin{aligned} L^*_{Vijk} &= 6\pi P_i P_j P_k \theta^{2/3} \left(\frac{2}{5} \left(\frac{16\pi^5}{243} \right)^{1/3} \Gamma(\frac{1}{3}) - \pi^2 (\frac{3}{4\pi})^{4/3} \frac{8}{27}\sqrt{3}\frac{\pi}{\Gamma\left(\frac{2}{3}\right)} \right) \quad (10) \\ &= 6\pi P_i P_j P_k \times 1.175\,6\theta^{2/3} \end{aligned}$$

4.2 Delaunay mosaic

The Delaunay tessellation is the dual of the Voronoï tessellation [2]. We have ([2], p. 384)

$$\begin{aligned} \overline{V}(C) &= \frac{35}{24\pi^2\theta} \\ \overline{b} &\simeq 1.118\theta^{-1/3} \end{aligned}$$

and therefore, if we neglect the term $r''(0)$, which is not available,

$$L^*_{Vijk} = 6\pi P_i P_j P_k 1.118\theta^{-1/3} \frac{48\pi^2}{35}\theta = 6\pi P_i P_j P_k 15.133\theta^{2/3} \qquad (11)$$

4.3 Poisson and STIT mosaics

Starting from a Poisson tessellation of space [13, 8] is generated a Poisson mosaic (Figure 2), each cell being a Poisson polyhedron. Similarly, from the construction of iterated tessellations (STIT model [16]), a tessellation with Poisson polyhedra in a different arrangement is obtained. Noting $\lambda = \lambda_3$ the intensity of Poisson hyperplanes generating the Poisson tessellation, we have:

$$\begin{aligned} \overline{V}(C) &= \frac{6}{\pi^4 \lambda^3} \\ \overline{b} &= \frac{3}{2\pi\lambda} \\ \frac{\overline{b}}{\overline{V}(C)} &= \frac{\pi^3 \lambda^2}{4} \end{aligned}$$

For this model,

$$\begin{aligned} r(h) &= \exp(-\pi\lambda h) \\ r'(h) &= -\pi\lambda \exp(-\pi\lambda h) \\ r''(h) &= \pi^2\lambda^2 \exp(-\pi\lambda h),\ r''(0) = \pi^2\lambda^2 \end{aligned}$$

and

$$L^*_{Vijk} = 6\pi P_i P_j P_k \pi^2 \lambda^2 (2\pi/4 - 1) = 6\pi P_i P_j P_k \pi^2 \lambda^2 0.570\,80 \qquad (12)$$

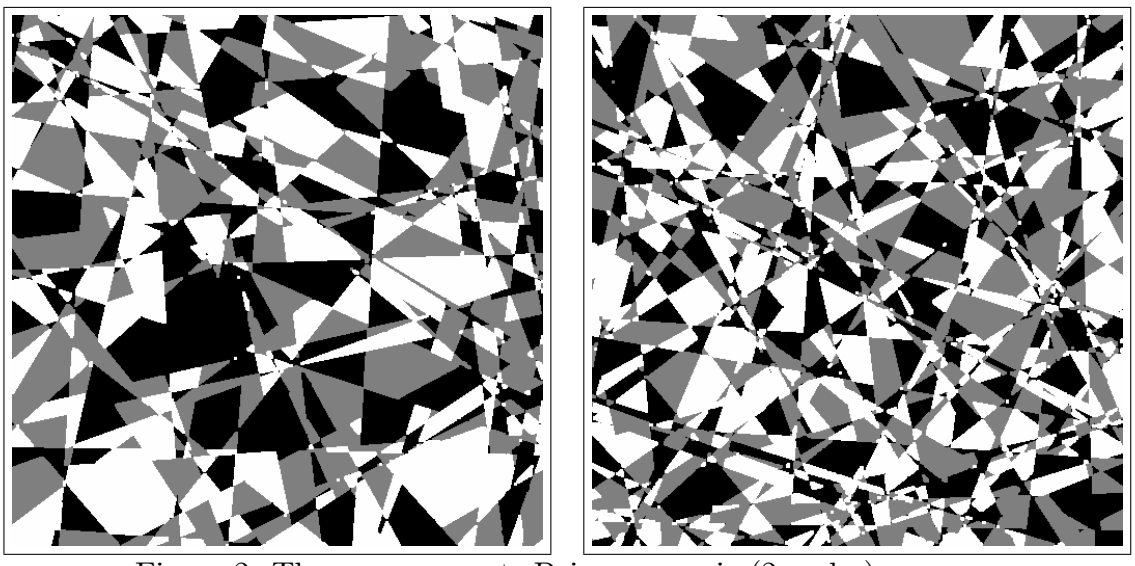

Figure 2: Three-components Poisson mosaic (2 scales)
left ($P_1 = 0.368$, $P_2 = 0.328$, $P_3 = 0.304$)
right ($P_1 = 0.353$, $P_2 = 0.35$, $P_3 = 0.297$)

4.4 Dead Leaves mosaic

The construction of the Dead Leaves Tessellation is obtained sequentially, as detailed in [12, 8]. By implantation of any shape of compact set A' (like spheres, ellipsoids, cylinders, Poisson polyhedra, etc.), random tessellations with cells of complex shapes are obtained. It was shown in that case:

$$\begin{aligned} s(h_1,h_2) &= \frac{\overline{V}(A' \cap A'_{-h_1} \cap A'_{-h_2})}{\overline{V}(A')} \frac{\overline{V}(A')}{\overline{V}(A' \cup A'_{-h_1} \cup A'_{-h_2})} \\ &= \frac{\zeta(h_1,h_2)}{\xi(h_1,h_2)} \end{aligned}$$

For this model, the normalized geometrical covariogram of a class of the tessellation $\rho(h)$ is given as a function of the normalized covariogram of the grains $r(h)$ by

$$\rho(h) = \frac{r(h)}{2 - r(h)}$$

and therefore

$$\begin{aligned} \rho'(h) &= \frac{2r'(h)}{(2-r(h))^2} \\ \rho'(0) &= 2r'(0) \end{aligned}$$

We have

$$\begin{aligned} \rho''(h) &= \frac{2\,(2-r(h))^2\, r''(h) + 2r'(h)2(2-r(h))r'(h)}{(2-r(h))^4} \\ \rho''(0) &= 2r''(0) + 4(r'(0))^2 \end{aligned}$$

$$\frac{\partial}{\partial h_1} s(h_1,h_2) = \frac{\xi(h_1,h_2)\frac{\partial}{\partial h_1}\zeta(h_1,h_2) - \zeta(h_1,h_2)\frac{\partial}{\partial h_1}\xi(h_1,h_2)}{(\xi(h_1,h_2))^2}$$

and

$$\left(\frac{\partial}{\partial h_1} s(h_1,h_2)\right)_{h_1=0,h_2=0} = \rho'(0) = 2r'(0) = r'(0) - \left(\frac{\partial}{\partial h_1}\xi(h_1,h_2)\right)_{h_1=0,h_2=0}$$

so that

$$\left(\frac{\partial}{\partial h_1}\xi(h_1,h_2)\right)_{h_1=0,h_2=0} = \left(\frac{\partial}{\partial h_2}\xi(h_1,h_2)\right)_{h_1=0,h_2=0} = -r'(0)$$

The second order derivative of $s(h_1, h_2)$ is given by (noting $\xi(h_1, h_2) = \xi$ and $\zeta(h_1, h_2) = \zeta$)

$$\begin{aligned} & \xi^4 \frac{\partial^2}{\partial h_1 \partial h_2} s(h_1, h_2) \qquad (13) \\ = \; & \xi^2 \left(\frac{\partial}{\partial h_2} \xi \frac{\partial}{\partial h_1} \zeta + \xi \frac{\partial^2}{\partial h_1 \partial h_2} \zeta - \frac{\partial}{\partial h_1} \xi \frac{\partial}{\partial h_2} \zeta - \zeta \frac{\partial^2}{\partial h_1 \partial h_2} \xi \right) - 2\xi \frac{\partial}{\partial h_2} \xi \left(\xi \frac{\partial}{\partial h_1} \zeta - \zeta \frac{\partial}{\partial h_1} \xi \right) \end{aligned}$$

We have

$$\xi(h_1, h_2) = 3 - r(h_1) - r(h_2) - r(h_3) + \zeta(h_1, h_2)$$

and then

$$\frac{\partial^2}{\partial h_1 \partial h_2} \xi = \frac{\partial^2}{\partial h_1 \partial h_2} \zeta - r''(h_3)$$

To evaluate $\left(\frac{\partial^2}{\partial h_1 \partial h_2} s(h_1, h_2) \right)_{h_1=0, h_2=0}$, we use equation (13) and the fact that $\left(\frac{\partial}{\partial h_i} \zeta \right)_{h_i=0} = r'(0)$. Therefore

$$\begin{aligned} & \left(\frac{\partial^2}{\partial h_1 \partial h_2} s(h_1, h_2) \right)_{h_1=0, h_2=0} \\ = \; & -(r'(0))^2 + \frac{\overline{b}}{\overline{V}(A')} + (r'(0))^2 - \frac{\overline{b}}{\overline{V}(A')} + r''(0) + 2r'(0) \left(r'(0) + r'(0) \right) \\ = \; & 4(r'(0))^2 - + r''(0) \end{aligned}$$

It comes

$$\begin{aligned} 2 \left(\frac{\partial^2 s(h_1, h_2)}{\partial h_1 \partial h_2} \right)_{h_1=0, h_2=0} - \rho''(0) &= 8(r'(0))^2 - 2r''(0) + 2r''(0) - 4(r'(0))^2 \\ &= 4(r'(0))^2 = 4 \left(\frac{\overline{S}(A')}{4\overline{V}(A')} \right)^2 = \frac{1}{4} \left(\frac{\overline{S}(A')}{\overline{V}(A')} \right)^2 \end{aligned}$$

where $\overline{S}(A')$ and $\overline{V}(A')$ are the average surface area and the average volume of the compact set A'. Finally equation (8) becomes for the Dead Leaves mosaic:

$$L^*_{Vijk} = 6\pi P_i P_j P_k \frac{1}{4} \left(\frac{\overline{S}(A')}{\overline{V}(A')} \right)^2 = \frac{3\pi}{2} P_i P_j P_k \left(\frac{\overline{S}(A')}{\overline{V}(A')} \right)^2 \qquad (14)$$

The term $(r'(0))^2$ satisfies

$$(r'(0))^2 = \frac{1}{\overline{L}^2}$$

where $\overline{L}$ is the average intercept of the primary grain A'. Therefore, the mean length of triple lines is inversely proportional to the square of a size parameter of the microstructure. Since $\rho'(0) = 2r'(0)$, the average intercept of the grain induced in the Dead Leaves Tessellation is twice the average intercept of the mosaic built on the same grains [12]. As a result, a factor of at least the order of 4 is expected for the mean length of triple lines of the Dead Leaves model wit the same grains. It is interesting to consider some instructive examples.

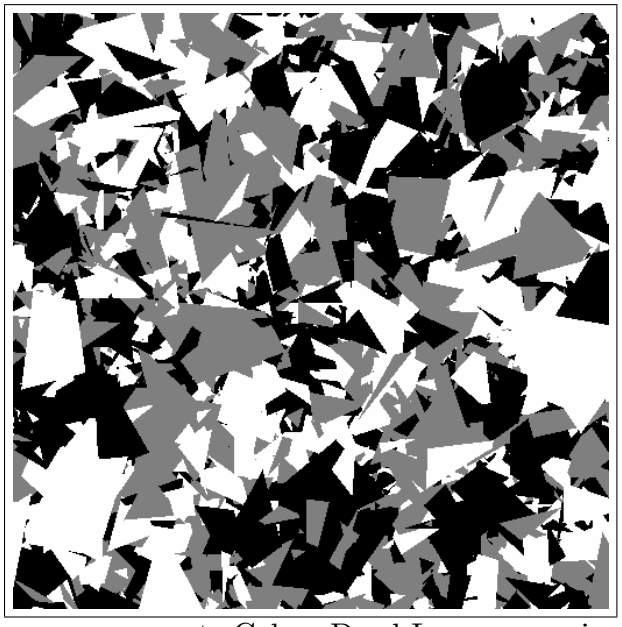

Figure 3: Three-components Colors Dead Leaves mosaic with Poisson primary grains ($P_1 = 0.345$, $P_2 = 0.32$, $P_3 = 0.335$)

- Using as primary grains Voronoï polyhedra with surface area $S \simeq 5.821\theta^{-2/3}$ [2], it comes $L^*_{Vijk} = \frac{3\pi}{2} P_i P_j P_k 33.884\theta^{2/3}$, to be compared to $L^*_{Vijk} = 6\pi P_i P_j P_k \times 1.1756\theta^{2/3}$ in the case of the Voronoï mosaic. The triple boundary line of the Voronoï Dead Leaves Tessellation is 7.20 times higher.

- Using Poisson polyhedra as primary grains (Figure 3), with surface area $24/(\pi^3\lambda^2)$ [13], we get $\frac{\overline{S}(A')}{\overline{V}(A')} = 4\pi\lambda$. It comes $L^*_{Vijk} = \frac{3\pi}{2} \times 16 P_i P_j P_k \pi^2 \lambda^2$ to be compared to $L^*_{Vijk} = 6\pi P_i P_j P_k \pi^2 \lambda^2 0.5708$ for the Poisson or the STIT mosaic. The triple boundary line of the Poisson Dead Leaves Tessellation is 7 times higher.

- Using Delaunay polyhedra, with surface area $S \simeq 2.389\theta^{-2/3}$ and $V = 35/(24\pi^2\theta)$ [2], it comes $L^*_{Vijk} = \frac{3\pi}{2} P_i P_j P_k (2.389\theta^{1/3} \frac{24\pi 2}{35})^2$, to be com-

pared to $6\pi P_i P_j P_k 15.133\theta^{2/3}$. The triple boundary line of the Delaunay Dead Leaves Tessellation is 1.75 times higher, but the length of the triple line of the Delaunay mosaic is largely over estimated.

The Dead Leaves mosaic generates more fragmented grains, providing much longer triple boundary lines (with a factor of the order of 7 in the studied examples) starting from the same initial grains.

5 Multi-components Color Dead Leaves

A more general model than the Dead Leaves mosaic is obtained by sequential implantation of color random grains $A'_i(t)$ with intensity $\theta_i(t)$, generating the Color Dead Leaves model [6, 7, 8]. For the present purpose, we consider the time homogeneous case, where the grains A'_i and the intensities θ_i do not depend on time. We presently consider a multi-components model A_i, A_j, A_k,...,A_m built from m types of grains A'_i, $i = 1, 2, 3, ..., m$ and intensities θ_i, $i = 1, 2, 3, \ ... \ m$. The process is stopped at $t = +\infty$. A realization of a 2D section of a 3D model is shown on Figure 4.

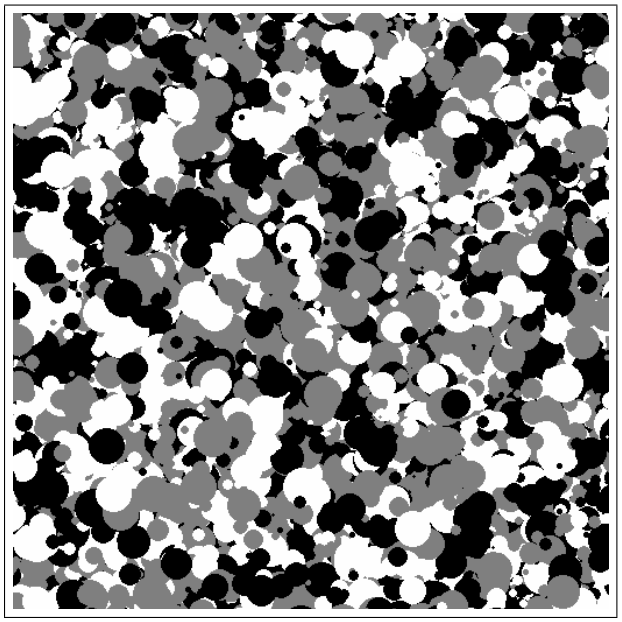

Figure 4: Three-components Colors Dead Leaves with spherical primary grains ($P_1 = 0.318$, $P_2 = 0.35$, $P_3 = 0.332$)

During the sequence, new occurring grains cover already present grains [6]. For the time homogeneous Color Dead Leaves model, the volume fraction

P_i of the set A_i for $t \to \infty$ is given by

$$P_i = \frac{\theta_i K_i(0)}{\sum\limits_{j=1}^{j=m} \theta_j K_j(0)}$$

Some third order moments are given in [6, 8], but here we have to derive probabilities $P_{ijk}(t)$ of any triplet $\{i, j, k\}$. The event

$$\{x \in A_i(t), x + h_1 \in A_j(t), x + h_2 \in A_k(t)\}$$

can be decomposed into a sequence of incompatible elementary events at different times $0 < u < t$:

i) at some time u, x covered by some grain A'_i, $x+h_1$ and $x+h_2$ uncovered by A'_i but $x + h_1 \in A_j(u), x + h_2 \in A_k(u)$ with probability $C_{jk}(h_3, u)$.

ii) From time u to t, points $x, x + h_1, x + h_2$ remain outside of grains appearing during this period, and building a sequential Boolean model, with probability $Q(h_1, h_2, u, t)$.

The elementary probability $P\{x \in A'_i(u), x + h_1 \notin A'_i(u), x + h_2 \notin A'_i(u)\}$ is given by

$$\begin{aligned} & P\{x \in A'_i(u), x + h_1 \notin A'_i(u), x + h_2 \notin A'_i(u)\} \\ = \; & \theta_i K_i(0) \left(1 - r_i(h_1) - r_i(h_2) + s_i(h_1, h_2)\right) du \end{aligned}$$

Considering similarly the coverage of $x + h_1$ by some $A'_j(u)$ and of $x + h_2$ by some $A'_k(u)$, we get after integration with respect to u

$$\begin{aligned} P_{ijk}(h_1, h_2, t) \; = \; & \int_0^t \theta_i K_i(0) \left(1 - r_i(h_1) - r_i(h_2) + s_i(h_1, h_2)\right) C_{jk}(h_3, u) Q(h_1, h_2, u, t) du \\ & + \int_0^t \theta_j K_j(0) \left(1 - r_j(h_1) - r_j(h_3) + s_j(h_1, h_2)\right) C_{ik}(h_2, u) Q(h_1, h_2, u, t) du \\ & + \int_0^t \theta_k K_k(0) \left(1 - r_k(h_2) - r_k(h_3) + s_k(h_1, h_2)\right) C_{ij}(h_1, u) Q(h_1, h_2, u, t) du \end{aligned}$$

with ([8], p. 358)

$$\begin{aligned} C_{ij}(h_1, u) &= P_i P_j \left[\frac{2 - r_i(h_1) - r_j(h_1)}{2 - r(h_1)} \left(1 - Q(h_1, u)\right) \right. \\ &\quad \left. - \frac{2 - r_i(h_1) - r_j(h_1)}{1 - r(h_1)} \left(q(u) - Q(h_1, u)\right) \right] \\ q(u) &= \exp\left(-\theta K(0) u\right) \\ Q(h_1, u) &= q(u)^{2 - r(h_1)} \end{aligned}$$

where

$$\begin{aligned}\theta K(0) &= \sum_{i=1}^{i=m} \theta_i K_i(0) \\ r(h_1) &= \sum_{i=1}^{i=m} P_i r_i(h)\end{aligned}$$

We have

$$Q(h_1, h_2, u, t) = \exp\left(-\theta K(0)(t-u)\xi(h_1, h_2)\right) = q(t-u)^{\xi(h_1,h_2)}$$

with

$$\xi(h_1, h_2) = \sum_{i=1}^{i=m} P_i \left(3 - r_i(h_1) - r_i(h_2) - r_i(h_3) + \zeta_i(h_1, h_2)\right)$$

and

$$\zeta_i(h_1, h_2) = \frac{\overline{V}(A'_i \cap A'_{i-h_1} \cap A'_{i-h_2})}{\overline{V}(A'_i)}$$

$$\int_0^t Q(h_1, h_2, u, t)du = \frac{1 - \exp\left(-\theta K(0) t \xi(h_1, h_2)\right)}{\theta K(0)\xi(h_1, h_2)}$$

$$\begin{aligned}\int_0^t Q(h, u)Q(h_1, h_2, u, t)du &= \int_0^t q(u)^{2-r(h)} q(t-u)^{\xi(h_1,h_2)} du \\ &= q(t)^{\xi(h_1,h_2)} \int_0^t \exp\left(-\theta K(0)\left(2 - r(h) - \xi(h_1, h_2)\right) u\right) du \\ &= \frac{q(t)^{\xi(h_1,h_2)}}{\theta K(0)\left(2 - r(h) - \xi(h_1, h_2)\right)} \left(1 - \frac{Q(h, t)}{q(t)^{\xi(h_1,h_2)}}\right) \\ &= \frac{q(t)^{\xi(h_1,h_2)} - Q(h, t)}{\theta K(0)\left(2 - r(h) - \xi(h_1, h_2)\right)}\end{aligned}$$

$$\int_0^t q(u)Q(h_1, h_2, u, t)du = \frac{q(t)^{\xi(h_1,h_2)} - q(t)}{\theta K(0)\left(1 - \xi(h_1, h_2)\right)}$$

As a consequence,

$$\begin{aligned}&\int_0^t C_{ij}(h_1, u)Q(h_1, h_2, u, t)du \\ = \; & P_i P_j \left[\frac{2 - r_i(h_1) - r_j(h_1)}{2 - r(h_1)} \left(\frac{1 - \exp\left(-\theta K(0) t \xi(h_1, h_2)\right)}{\theta K(0)\xi(h_1, h_2)} - \frac{q(t)^{\xi(h_1,h_2)} - q(t)}{\theta K(0)\left(1 - \xi(h_1, h_2)\right)}\right)\right. \\ & \left. - \frac{2 - r_i(h_1) - r_j(h_1)}{1 - r(h_1)} \left(\frac{q(t)^{\xi(h_1,h_2)} - q(t)}{\theta K(0)\left(1 - \xi(h_1, h_2)\right)} - \frac{q(t)^{\xi(h_1,h_2)} - Q(h_1, t)}{\theta K(0)\left(2 - r(h_1) - \xi(h_1, h_2)\right)}\right)\right]\end{aligned}$$

When $t \to \infty$, $q(t) \to 0$ and $Q(h_1, t) \to 0$ and therefore,

$$\int_0^\infty C_{ij}(h_1, u) Q(h_1, h_2, u, t) du = \frac{P_i P_j}{\theta K(0) \xi(h_1, h_2)} \left(\frac{2 - r_i(h_1) - r_j(h_1)}{2 - r(h_1)} \right)$$

and

$$\begin{aligned} & P_{ijk}(h_1, h_2) \frac{\xi(h_1, h_2)}{P_i P_j P_k} \qquad (15) \\ = \; & (1 - r_i(h_1) - r_i(h_2) + s_i(h_1, h_2)) \frac{2 - r_j(h_3) - r_k(h_3)}{2 - r(h_3)} \\ & + (1 - r_j(h_1) - r_j(h_3) + s_j(h_1, h_2)) \frac{(2 - r_i(h_2) - r_k(h_2)}{2 - r(h_2)} \\ & + (1 - r_k(h_2) - r_k(h_3) + s_k(h_1, h_2)) \frac{(2 - r_i(h_1) - r_j(h_1)}{2 - r(h_1)} \end{aligned}$$

A particular case is obtained when using the same primary grains for each component. It corresponds to the Dead Leaves mosaic. In that case,

$$\begin{aligned} r(h) &= r_i(h) = r_j(h) = r_k(h) \\ s_i(h_1, h_2) &= s_j(h_1, h_2) = s_k(h_1, h_2) = s(h_1, h_2) \end{aligned}$$

so that equation (15) becomes:

$$\begin{aligned} & P_{ijk}(h_1, h_2) \frac{\xi(h_1, h_2)}{P_i P_j P_k} \\ = \; & 2 (1 - r(h_1) - r(h_2) + s(h_1, h_2)) \frac{1 - r(h_3)}{2 - r(h_3)} \\ & + 2 (1 - r(h_1) - r(h_3) + s(h_1, h_2)) \frac{1 - r(h_2)}{2 - r(h_2)} \\ & + 2 (1 - r(h_2) - r(h_3) + s(h_1, h_2)) \frac{1 - r(h_1)}{2 - r(h_1)} \end{aligned}$$

and we can check that the formula given by equation (6) is recovered. Lengthy computations are simplified when $|h_1| = |h_2| = h_3 = h$, for which it

comes for equation (15):

$$\begin{aligned}
& P_{ijk}(h_1,h_2)\frac{\xi(h_1,h_2)}{P_iP_jP_k} \\
= \;& 2\left(1-r(h)-r(h)+s(h_1,h_2)\right)\frac{1-r(h)}{2-r(h)} \\
& +2\left(1-r(h)-r(h)+s(h_1,h_2)\right)\frac{1-r(h)}{2-r(h)} \\
& +2\left(1-r(h)-r(h)+s(h_1,h_2)\right)\frac{1-r(h)}{2-r(h)} \\
= \;& 2\left(1-2r(h)+s(h_1,h_2)\right)3\frac{1-r(h)}{2-r(h)}
\end{aligned}$$

For the result derived from the Dead Leaves mosaic, we get:

$$\begin{aligned}
& P_{ijk}(h_1,h_2)\frac{\xi(h_1,h_2)}{P_iP_jP_k} \\
= \;& (3-3r(h)+s(h_1,h_2))\left(1-\frac{3r(h)}{2-r(h)}\right)+2s(h_1,h_2) \\
= \;& (3(1-r(h))+s(h_1,h_2))\,2\left(\frac{1-2r(h)}{2-r(h)}\right)+2s(h_1,h_2) \\
= \;& \frac{2}{2-r(h)}\left(s(h_1,h_2)(1-2r(h)+2-r(h))+6(1-r(h))(1-2r(h))\right) \\
= \;& \frac{6(1-r(h))}{2-r(h)}\left(s(h_1,h_2)+1-2r(h)\right)
\end{aligned}$$

providing the same result.

To compute $\frac{\partial^2}{\partial h_1 \partial h_2}P_{ijk}(h_1,h_2)$, we start from equation (15) and take into account that many terms are equal to zero when $h_1 = h_2$. We get

$$\begin{aligned}
& \frac{\partial}{\partial h_1}\left[(1-r_i(h_1)-r_i(h_2)+s_i(h_1,h_2))\right]_{h_1=0,h_2=0} \\
= \;& \frac{\partial}{\partial h_2}\left[(1-r_i(h_1)-r_i(h_2)+s_i(h_1,h_2))\right]_{h_2=0,h_1=0} = 0
\end{aligned}$$

$$\begin{aligned}
\frac{\partial}{\partial h_1}\left[(1-r_j(h_1)-r_j(h_3)+s_j(h_1,h_2))\right]_{h_1=0h_2=0} &= -r_j'(0) \\
\frac{\partial}{\partial h_2}\left[(1-r_j(h_1)-r_j(h_3)+s_j(h_1,h_2))\right]_{h_1=0h_2=0} &= 0
\end{aligned}$$

and

$$\begin{aligned}
\frac{\partial}{\partial h_1}\left[\frac{(2-r_i(h_2)-r_k(h_2)}{2-r(h_2)}\right] &= 0 \\
\frac{\partial}{\partial h_2}\left[\frac{(2-r_i(h_2)-r_k(h_2)}{2-r(h_2)}\right] &= -\frac{(2-r(h_2))((r_i'(h_2)+r_k'(h_2))}{(2-r(h_2))^2} \\
&\quad -\frac{r'(h_2)((2-r_i(h_2)-r_k(h_2))}{(2-r(h_2))^2} \\
\frac{\partial}{\partial h_2}\left[\frac{(2-r_i(h_2)-r_k(h_2)}{2-r(h_2)}\right]_{h_2=0} &= -r_i'(0)-r_k'(0)
\end{aligned}$$

For the last term,

$$\begin{aligned}
\frac{\partial}{\partial h_1}\left[(1-r_k(h_2)-r_k(h_3)+s_k(h_1,h_2))\right]_{h_1=0h_2=0} &= 0 \\
\frac{\partial}{\partial h_2}\left[(1-r_k(h_2)-r_k(h_3)+s_k(h_1,h_2))\right]_{h_1=0h_2=0} &= -r_k'(0)
\end{aligned}$$

and

$$\begin{aligned}
\frac{\partial}{\partial h_1}\left[\frac{(2-r_i(h_1)-r_j(h_1)}{2-r(h_1)}\right]_{h_1=0} &= -r_i'(0)-r_j'(0) \\
\frac{\partial}{\partial h_2}\left[\frac{(2-r_i(h_1)-r_j(h_1)}{2-r(h_1)}\right] &= 0
\end{aligned}$$

Regrouping all non zero terms, we have

$$\begin{aligned}
&\frac{\partial^2}{\partial h_1 \partial h_2}\left[P_{ijk}(h_1,h_2)\frac{\xi(h_1,h_2)}{P_iP_jP_k}\right]_{h_1=0,h_2=0} \\
&= r_j'(0)(r_i'(0)+r_k'(0))+r_k'(0)(r_i'(0)+r_j'(0)) \\
&= r_j'(0)r_i'(0)+r_k'(0)r_i'(0)+2r_k'(0)r_j'(0)
\end{aligned}$$

Applying the second order derivative to the first term of the previous equation,

$$\begin{aligned}
&\frac{\partial^2}{\partial h_1 \partial h_2}\left[P_{ijk}(h_1,h_2)\xi(h_1,h_2)\right] \\
&= \frac{\partial^2}{\partial h_1 \partial h_2}\left[P_{ijk}(h_1,h_2)\right]\xi+\frac{\partial}{\partial h_1}\left[P_{ijk}(h_1,h_2)\right]\frac{\partial \xi}{\partial h_2}+\frac{\partial}{\partial h_2}\left[P_{ijk}(h_1,h_2)\right]\frac{\partial \xi}{\partial h_1}
\end{aligned}$$

We have

$$\begin{aligned}
\frac{\partial}{\partial h_1}\left[P_{ijk}(h_1,h_2)\right]_{h_1=0,h_2=0} &= 0 \\
\frac{\partial}{\partial h_2}\left[P_{ijk}(h_1,h_2)\right]_{h_1=0,h_2=0} &= 0
\end{aligned}$$

and

$$\begin{aligned}
&\frac{\partial^2}{\partial h_1 \partial h_2}\left[P_{ijk}(h_1,h_2))\frac{\xi(h_1,h_2)}{P_iP_jP_k}\right]_{h_1=0,h_2=0}\\
=\;&\frac{1}{P_iP_jP_k}\left[\frac{\partial^2}{\partial h_1 \partial h_2}\left[P_{ijk}(h_1,h_2)\right]_{h_1=0,h_2=0}\right]\\
=\;&\left(r'_i(0)r'_j(0)+r'_i(0)r'_k(0)+2r'_k(0)r'_j(0)\right)
\end{aligned}$$

By permutations of the indices i, j, k, we obtain two other values for the second order partial derivatives. Combining them, and summing, we get

$$\begin{aligned}
L^*_{Vijk} \;=\;&\\
&2\pi P_iP_jP_k\left(\left(r'_i(0)r'_j(0)+r'_i(0)r'_k(0)+2r'_k(0)r'_j(0)\right)\right.\\
&+\left((r'_k(0)r'_i(0))+r'_k(0)r'_j(0)+2r'_i(0)r'_j(0)\right)\\
&\left.+\left(r'_i(0)r'_j(0)+r'_j(0)r'_k(0)+2r'_i(0)r'_k(0)\right)\right)\\
=\;&\frac{\pi}{8}P_iP_jP_k\left(r'_i(0)r'_j(0)+r'_i(0)r'_k(0)+r'_k(0)r'_j(0)\right)
\end{aligned}$$

and therefore

$$\begin{aligned}
&L^*_{Vijk} \qquad (16)\\
=\;&\frac{\pi}{8}\frac{64}{16}P_iP_jP_k\left(\left(\frac{\overline{S}(A'_i)}{\overline{V}(A'_i)}\right)\left(\frac{\overline{S}(A'_j)}{\overline{V}(A'_j)}\right)+\left(\frac{\overline{S}(A'_i)}{\overline{V}(A'_i)}\right)\left(\frac{\overline{S}(A'_k)}{\overline{V}(A'_k)}\right)+\left(\frac{\overline{S}(A'_k)}{\overline{V}(A'_k)}\right)\left(\frac{\overline{S}(A'_j)}{\overline{V}(A'_j)}\right)\right)\\
=\;&\frac{\pi}{2}P_iP_jP_k\left(\left(\frac{\overline{S}(A'_i)}{\overline{V}(A'_i)}\right)\left(\frac{\overline{S}(A'_j)}{\overline{V}(A'_j)}\right)+\left(\frac{\overline{S}(A'_i)}{\overline{V}(A'_i)}\right)\left(\frac{\overline{S}(A'_k)}{\overline{V}(A'_k)}\right)+\left(\frac{\overline{S}(A'_k)}{\overline{V}(A'_k)}\right)\left(\frac{\overline{S}(A'_j)}{\overline{V}(A'_j)}\right)\right)
\end{aligned}$$

For given primary grains A_i, A_j and A_k, the optimal composition, maximizing L_{Vijk}, is provided by $P_i = P_j = P_k = 1/3$, as for the mosaic model.

When using the same primary grains for components A_i, A_j and A_k, the three-components Color Dead Leaves becomes a Dead Leaves mosaic, and we obtain:

$$L^*_{Vijk} = \frac{3\pi}{2}\left(\frac{\overline{S}(A')}{\overline{V}(A')}\right)^2 P_iP_jP_k \qquad (17)$$

This estimate recovers the result obtained from the Dead Leaves mosaic given by equation (14).

It is interesting to express L^*_{Vijk} in equation (16) as a function of the volume fractions and of the specific areas of contacts between components A_i, A_j, $S_{V_{ij}}$. Noting $\frac{\overline{S}(A'_i)}{\overline{V}(A'_i)} = a_i$, we have ([6, 8], p. 359):

$$\begin{aligned}
S_{V_{ij}} &= P_iP_j(a_i+a_j)\\
S_{V_{ik}} &= P_iP_k(a_i+a_k)\\
S_{V_{jk}} &= P_jP_k(a_j+a_k)
\end{aligned}$$

We get

$$\left(\frac{S_{V_{ij}}}{P_iP_j}\right)^2+\left(\frac{S_{V_{ik}}}{P_iP_k}\right)^2+\left(\frac{S_{V_{jk}}}{P_jP_k}\right)^2=(a_i+a_j)^2+(a_i+a_k)^2+(a_j+a_k)^2 \quad (18)$$

We have:

$$\begin{aligned}\frac{S_{V_{ij}}}{P_iP_j}-\frac{S_{V_{ik}}}{P_iP_k} &= a_j-a_k \quad (19)\\ \frac{S_{V_{ij}}}{P_iP_j}-\frac{S_{V_{jk}}}{P_jP_k} &= a_i-a_k\\ \frac{S_{V_{ik}}}{P_iP_k}-\frac{S_{V_{jk}}}{P_jP_k} &= a_i-a_j\end{aligned}$$

Combining equations (18) and (19), we get:

$$\begin{aligned}&\left(\frac{S_{V_{ij}}}{P_iP_j}\right)^2+\left(\frac{S_{V_{ik}}}{P_iP_k}\right)^2+\left(\frac{S_{V_{jk}}}{P_jP_k}\right)^2-\left(\frac{S_{V_{ij}}}{P_iP_j}-\frac{S_{V_{ik}}}{P_iP_k}\right)^2\\ &-\left(\frac{S_{V_{ij}}}{P_iP_j}-\frac{S_{V_{jk}}}{P_jP_k}\right)^2-\left(\frac{S_{V_{ik}}}{P_iP_k}-\frac{S_{V_{jk}}}{P_jP_k}\right)^2\\ =\;&(a_i+a_j)^2+(a_i+a_k)^2+(a_j+a_k)^2-(a_j-a_k)^2-(a_i-a_k)^2-(a_i-a_j)^2\\ =\;&4(a_ia_j+a_ia_k+a_j+a_k)\end{aligned}$$

Equation (16) can be rewritten

$$\begin{aligned}L^*_{Vijk} &= \frac{\pi}{8}P_iP_jP_k\left(\left(\frac{S_{V_{ij}}}{P_iP_j}\right)^2+\left(\frac{S_{V_{ik}}}{P_iP_k}\right)^2+\left(\frac{S_{V_{jk}}}{P_jP_k}\right)^2\right) \quad (20)\\ &-\frac{\pi}{8}P_iP_jP_k\left(\left(\frac{S_{V_{ij}}}{P_iP_j}-\frac{S_{V_{ik}}}{P_iP_k}\right)^2+\left(\frac{S_{V_{ij}}}{P_iP_j}-\frac{S_{V_{jk}}}{P_jP_k}\right)^2+\left(\frac{S_{V_{ik}}}{P_iP_k}-\frac{S_{V_{jk}}}{P_jP_k}\right)^2\right)\end{aligned}$$

Alternatively, equation (16) can be expressed as a function of specific surface areas of all components A_i. We have ([6, 8], p. 359):

$$\begin{aligned}S_{V_i} &= P_i\left((1-2P_i)\left(\frac{\overline{S}(A'_i)}{\overline{V}(A'_i)}\right)+\frac{S}{K(0)}\right)\\ &= P_i\left((1-2P_i)\,a_i+a\right)\end{aligned}$$

from which we obtain

$$\begin{aligned}S_{V_i}-P_ia &= (1-2P_i)\,a_i\\ a_i &= \frac{S_{V_i}-P_ia}{1-2P_i}\end{aligned}$$

with

$$\begin{aligned} S &= \sum_{i=1}^{i=m} \theta_i \frac{\overline{S}(A'_i)}{\sum_{i=1}^{i=m} \theta_i} \\ a &= \frac{\sum_{i=1}^{i=m} \theta_i \overline{S}(A'_i)}{\sum_{i=1}^{i=m} \theta_i K_i(0)} = \frac{\sum_{i=1}^{i=m} \theta_i K_i(0) \frac{\overline{S}(A'_i)}{K_i(0)}}{\sum_{i=1}^{i=m} \theta_i K_i(0)} = \sum_{i=1}^{i=m} P_i a_i \\ &= \sum_{i=1}^{i=m} \frac{P_i S_{V_i}}{1-2P_i} - a \sum_{i=1}^{i=m} \frac{P_i^2}{1-2P_i} \end{aligned}$$

Therefore,

$$a \left(1 + \sum_{i=1}^{i=m} \frac{P_i^2}{1-2P_i} \right) = \sum_{i=1}^{i=m} \frac{P_i S_{V_i}}{1-2P_i}$$

and finally a is expressed as a function of volume fractions P_i and specific surface areas S_{V_i} by:

$$a = \frac{\sum_{i=1}^{i=m} \frac{P_i S_{V_i}}{1-2P_i}}{1 + \sum_{i=1}^{i=m} \frac{P_i^2}{1-2P_i}} \tag{21}$$

and equation (16) can be rewritten, with given by equation (21):

$$\begin{aligned} L^*_{Vijk} &= \\ & \frac{\pi}{2} P_i P_j P_k \left(\left(\frac{S_{V_i} - aP_i}{1-2P_i} \right) \left(\frac{S_{V_j} - aP_j}{1-2P_j} \right) \right. \\ & \left. + \left(\frac{S_{V_i} - aP_i}{1-2P_i} \right) \left(\frac{S_{V_k} - aP_k}{1-2P_k} \right) + \left(\frac{S_{V_k} - aP_k}{1-2P_k} \right) \left(\frac{S_{V_j} - aP_j}{1-2P_j} \right) \right) \end{aligned} \tag{22}$$

The merit of equations (20) and (22) is that in the framework of this model, L^*_{Vijk} is directly estimated from the volume fractions and specific surfaces areas of contact between $\{i, j, k\}$ components (equations (20)), or specific surface areas of all components (equation ((22)). This information is available from 2D (or even 1D) images of a microstructure by derivatives of the cross-covariances and covariances for $h = 0$, so that there is no needs to make an identification of the parameters of the underlying Color Dead Leaves model to provide an estimation of L^*_{Vijk} in that situation. Of course, a validation of the model to represent a given microstructure should be made, which is feasible from the use of covariances and cross-covariances.

6 Three components models based on the superposition of independent random sets

A convenient way to generate muti-component random structures is by means of a superposition of independent random sets, as initiated in [5, 6]. Consider now the random structure composed of $A_1 = A'_1$, $A_2 = A'_2 \cap (A_1)^c = A'_2 \cap (A'_1)^c$, and $A_3 = (A'_2)^c \cap (A'_1)^c$. The primary random sets A'_1, A'_2 are independent random sets. The probabilistic properties of each component A_i depend only on the probabilistic properties of the primary random sets A'_1 and A'_2. The TPB lines are obtained from the intersection of the boundaries of $A_1$and A_2, which are given by the intersection of the boundaries of $A'_1$and A'_2.

We denote by $k'_1(x)$ and $k'_2(x)$ the indicator functions of the sets A'_1 and A'_2. For this construction of three-components random sets, we will have to compute separately $P_{ijk}(h_1, h_2)$ for the six combinations of items $\{1, 2, 3\}$.

$$\begin{aligned} P_{123}(h_1,h_2) &= P(x \in A_1, x+h_1 \in A_2, x+h_2 \in A_3) \\ &= E\left\{k'_1(x)k'_2(x+h_1)(1-k'_1(x+h_1))(1-k'_2(x+h_2))(1-k'_1(x+h_2))\right\} \\ &= (q'_2 - Q'_2(h_3))E\left\{k'_1(x)(1-k'_1(x+h_1))(1-k'_1(x+h_2))\right\} \\ &= (q'_2 - Q'_2(h_3))\left(P'_1 - C'_1(h_1) - C'_1(h_2) + P'_1(h_1,h_2)\right) \end{aligned}$$

where $Q'_2(h_3)$ is the covariances of the set $(A'_2)^c$, and $P'_1(h_1, h_2)$ is the third order probability of the set A'_1. We have

$$\left(\frac{\partial}{\partial h_1}(q'_2 - Q'_2(h_3))\right)_{h_1=0} = \left(\frac{\partial}{\partial h_2}(q'_2 - Q'_2(h_3))\right)_{h_2=0} = -\left(C'_2(0)\right)'$$

and

$$\frac{\partial}{\partial h_1}(P'_1(h_1,h_2))_{h_1=0,h_2=0} = \frac{\partial}{\partial h_2}\left(P'_1(h_1,h_2)\right)_{h_1=0,h_2=0} = \left(C'_1(0)\right)'$$

When $h_1 = h_2 = h$ and $h \to 0$

$$\begin{aligned} & \left(\frac{\partial^2}{\partial h_1 \partial h_2} P_{123}(h_1,h_2)\right)_{h_1=0,h_2=0} \\ = & -\left(C'_2(0)\right)'\left(-\left(C'_1(0)\right)' + \frac{\partial}{\partial h_1}(P'_1(h_1,h_2))_{h_1=0,h_2=0}\right) \\ & -\left(C'_2(0)\right)'\left(-\left(C'_2(0)\right)' + \frac{\partial}{\partial h_2}(P'_1(h_1,h_2))_{h_1=0,h_2=0}\right) \\ = & \ 0 \end{aligned}$$

$$
\begin{aligned}
P_{231}(h_1,h_2) &= P(x\in A_2, x+h_1\in A_3, x+h_2\in A_1)\\
&= E\left\{k_2'(x)(1-k_1'(x))(1-k_2'(x+h_1))(1-k_1'(x+h_1))k_1'(x+h_2)\right\}\\
&= (q_2'-Q_2'(h_1))E\left\{k_1'(x+h_2)(1-k_1'(x))(1-k_1'(x+h_1))\right\}\\
&= (q_2'-Q_2'(h_1))\left(P_1'-C_1'(h_3)-C_1'(h_2)+P_1'(h_1,h_2)\right)
\end{aligned}
$$

and

$$
\begin{aligned}
&\left(\frac{\partial^2}{\partial h_1\partial h_2}P_{231}(h_1,h_2)\right)_{h_1=0,h_2=0}\\
&= -\left(C_2'(0)\right)'\left(-(C_1'(0))'-(C_1'(0))'+(C_1'(0))'\right)\\
&= \left(C_2'(0)\right)'\left(C_1'(0)\right)'
\end{aligned}
$$

$$
\begin{aligned}
P_{312}(h_1,h_2) &= P(x\in A_3, x+h_1\in A_1, x+h_2\in A_2)\\
&= E\left\{(1-k_1'(x))(1-k_2'(x))k_1'(x+h_1)(1-k_1'(x+h_2))(1-k_2'(x+h_2))\right\}\\
&= (q_2'-Q_2'(h_2))\left(P_1'-C_1'(h_1)-C_1'(h_3)+P_1'(h_1,h_2)\right)
\end{aligned}
$$

and

$$
\begin{aligned}
&\left(\frac{\partial^2}{\partial h_1\partial h_2}P_{312}(h_1,h_2)\right)_{h_1=0,h_2=0}\\
&= -\left(C_2'(0)\right)'\left(-(C_1'(0))'-(C_1'(0))'+(C_1'(0))'\right)\\
&= \left(C_2'(0)\right)'\left(C_1'(0)\right)'
\end{aligned}
$$

$$
\begin{aligned}
P_{213}(h_1,h_2) &= P(x\in A_2, x+h_1\in A_1, x+h_2\in A_3)\\
&= E\left\{(1-k_1'(x))k_2'(x)k_1'(x+h_1)(1-k_1'(x+h_2))(1-k_2'(x+h_2))\right\}\\
&= (q_2'-Q_2'(h_2))\left((P_1'-C_1'(h_1)-C_1'(h_3)+P_1'(h_1,h_2))\right)
\end{aligned}
$$

and

$$
\begin{aligned}
&\left(\frac{\partial^2}{\partial h_1\partial h_2}P_{213}(h_1,h_2)\right)_{h_1=0,h_2=0}\\
&= -\left(C_2'(0)\right)'\left(-(C_1'(0))'-(C_1'(0))'+(C_1'(0))'\right)\\
&= \left(C_2'(0)\right)'\left(C_1'(0)\right)'
\end{aligned}
$$

$$
\begin{aligned}
P_{132}(h_1,h_2) &= P(x\in A_1, x+h_1\in A_3, x+h_2\in A_2)\\
&= E\left\{k_1'(x)(1-k_1'(x+h_1))(1-k_2'(x+h_1))(1-k_1'(x+h_2))k_2'(x+h_2)\right\}\\
&= (q_2'-Q_2'(h_3))\left((P_1'-C_1'(h_1)-C_1'(h_2)+P_1'(h_1,h_2))\right)
\end{aligned}
$$

and

$$\left(\frac{\partial^2}{\partial h_1 \partial h_2} P_{132}(h_1, h_2)\right)_{h_1=0, h_2=0} = 0$$

$$\begin{aligned} P_{321}(h_1, h_2) &= P(x \in A_3, x + h_1 \in A_2, x + h_2 \in A_1) \\ &= E\left\{(1 - k_1'(x))(1 - k_2'(x))(1 - k_1'(x + h_1))k_2'(x + h_1)k_1'(x + h_2))\right\} \\ &= (q_2' - Q_2'(h_1))\left((P_1' - C_1'(h_2) - C_1'(h_3) + P_1'(h_1, h_2))\right) \end{aligned}$$

and

$$\begin{aligned} &\left(\frac{\partial^2}{\partial h_1 \partial h_2} P_{321}(h_1, h_2)\right)_{h_1=0, h_2=0} \\ &= -\left(C_2'(0)\right)'\left(-(C_1'(0))' - (C_1'(0))' + (C_1'(0))'\right) \\ &= \left(C_2'(0)\right)'\left(C_1'(0)\right)' \end{aligned}$$

and finally, noting S_{V1}' and S_{V2}' the specific surface areas of the random sets A_1' and A_2', we get

$$L_{V123}^* \simeq 8\left(C_2'(0)\right)'\left(C_1'(0)\right)' = \frac{1}{2} S_{V1}' S_{V2}' \tag{23}$$

We will now use for comparison a result from Stochastic Geometry giving L_{V123} when A_1', $A_2^{'}$ are independent random sets with specific surface areas S_{V1}' and S_{V2}' [14], [2]:

$$L_{V123} = \frac{\pi}{4} S_{V1}' S_{V2}' \tag{24}$$

The result of equation (24) shows that the value of L_{V123}^* given by equation 23 obtained by means of the third order moment $P_{ijk}(h_1, h_2)$ through equation (2) is underestimated. This bias is therefore corrected after multiplication of equation (2) by the factor $\frac{\pi}{2}$ to provide a correct estimation.

L_{V123}^* in equation (24) can also be expressed as a function of the specific surface areas of the observed sets A_1 and $A_2 = A_2^{'} \cap (A_1)^c$. We have

$$C_2(h) = C_2'(h) Q_1(h)$$

and therefore:

$$C_2'(0) = (1 - P_1)\left(C_2'(0)\right)' - C_1'(0) P_2'$$

$$S_{V2} = (1 - P_1) S_{V2}' + \frac{P_2}{1 - P_1} S_{V1}$$

and

$$S_{V2}' = \frac{S_{V2}}{1 - P_1} - \frac{P_2}{(1 - P_1)^2} S_{V1}$$

Equation (24) can be rewritten:

$$L^*_{V123} = \frac{2S_{V1}}{1-P_1}\left(S_{V2} - \frac{P_2}{1-P_1}S_{V1}\right) \tag{25}$$

L^*_{V123} can be directly estimated by equation (25) from the properties of the observed microstructure (volume fractions P_1, P_2 and specific surface areas S_{V1}, and S_{V2}) estimated on 1D or 2D images , without any identification of a random set model for the two components A_1 and A_2. The only condition for equation (25) to be valid is the assumption of independence of the two underlying random sets A_1 and A'_2, which can be easily tested from the experimental cross covariances ([8], p. 126). However, experimental sampling errors on the volume fractions and specific surface areas of components A_1 and A_2 can lead to large errors on L^*_{V123} estimated by equation (25).

The other specific surface areas are derived from the covariances and cross covariances of this model ([8], p. 125-126) and can be used for further tests of the assumption of independence:

$$\begin{aligned} S_{V3} &= (1-P_1)S'_{V2} + \frac{P_3}{1-P_1}S_{V1} = S_{V2} + \frac{P_3-P_2}{1-P_1}S_{V1} \\ S_{V_{12}} &= \frac{P_2}{1-P_1}S_{V1},\ S_{V_{13}} = \frac{P_3}{1-P_1}S_{V1},\ S_{V_{23}} = \frac{P_2}{1-P_1}S_{V1} - S_{V2} \end{aligned}$$

In what follows, we give examples of applications using the superposition of Boolean models, two-components mosaics, Color Dead Leaves models, a Dilution random function and truncated Gaussian random functions. The choice of a given model for the components A_1 and A_2 can be made separately among available models, which gives a lot of flexibility for the final microstructures and the corresponding lengths of TPB lines.

6.1 Superposition of Boolean models

In the case where the random sets A'_1 and A'_2 are Boolean random sets (Figure 5) with primary grains A'_i and with volume fraction $1-q_i$, we have ([8], p. 169):

$$S_{Vi} = -\frac{\overline{S}(A'_i)}{\overline{V}(A'_i)} q_i \log q_i$$

and therefore

$$L^*_{V123} = \frac{\pi}{4}\frac{\overline{S}(A'_1)}{\overline{V}(A'_1)}\frac{\overline{S}(A'_2)}{\overline{V}(A'_2)}(1-P_1)\log(1-P_1)(1-P'_2)\log(1-P'_2) \tag{26}$$

In a first step, it is interesting to look for volume fractions P_1 and P_2 maximizing L_{V123} for fixed primary grains. We have:

$$\begin{aligned}\frac{\partial}{\partial P_1}(1-P_1)\log(1-P_1) &= -1-\log(1-P_1)=0\\ 1-P_1 &= \exp -1,\ P_1 = 1-\exp -1 \simeq 0.632\,12\end{aligned}$$

and then for the variation with respect to P_2' we get

$$\begin{aligned}P_2' &= 1-\exp -1\\ P_2 &= \exp -1-\exp -2 \simeq 0.232\,54\end{aligned}$$

and

$$P_3 = 1-P_1-P_2 = \exp -2 \simeq 0.135\,34$$

We have to notice that the volume fractions P_1, P_2, and P_3 are larger than the usual percolation threshold of the Boolean model (A_1) and of its complementary set (like A_3). It is therefore expected that the TPB lines percolate in that case. They differ from the equirepartition maximizing L^*_{V123} in the case of the mosaic model.

For volume fractions maximizing L_{V123}, we have

$$\begin{aligned}(1-P_1)\log(1-P_1) &= -\exp -1\\ (1-P_1)\log(1-P_1)(1-P_2')\log(1-P_2') &= \exp -2 = 0.13534\end{aligned}$$

and equation (26) becomes

$$L^*_{V123\,\max} = \frac{\pi}{4}\frac{\overline{S}(A_1')}{\overline{V}(A_1')}\frac{\overline{S}(A_2')}{\overline{V}(A_2')}\exp -2 \simeq 0.10\,63\frac{\overline{S}(A_1')}{\overline{V}(A_1')}\frac{\overline{S}(A_2')}{\overline{V}(A_2')}$$

We can notice that $\frac{\overline{S}(A_i')}{\overline{V}(A_i')}$ in equation (26), is equal to $-4r_i'(0) = \frac{1}{\overline{L}_i}$, $\overline{L}_i$ being the average intercept of the grain A_i', which is a size parameter. As a consequence, L_{V123} decreases with $\overline{L}$ and is expected to increase for lower size of primary grains and given volume fractions of components.

For applications, it is interesting to collect the ratio $\frac{\overline{S}(A')}{\overline{V}(A')}$ for different types of grains. They are given in table 1 (where P mean Polyhedron).

Poisson fibres with radius r can be constructed as a limiting case of a Boolean model of cylinders for $l \to \infty$ and an intensity $\theta \to 0$ ([8], p. 224). For this model, we get:

$$\frac{S}{V} = \lim_{l\to\infty}\frac{2\pi r l}{\pi r^2 l} = \frac{2}{r}$$

	Sphere	Cylinder	Cube	Parallelepiped	Poisson P	Voronoï P	Delaunay P
S	$4\pi r^2$	$2\pi r(r+l)$	$6a^2$	$2(ab+bc+ca)$	$24/(\pi^3\lambda^2)$	$5.821\theta^{-2/3}$	$2.389\theta^{-2/3}$
V	$\frac{4}{3}\pi r^3$	$\pi r^2 l$	a^3	abc	$6/(\pi^4\lambda^3)$	$1/\theta$	$35/(24\pi^2\theta)$
S/V	$3/r$	$\frac{2(r+l)}{rl}$	$6/a$	$2(\frac{1}{a}+\frac{1}{b}+\frac{1}{c})$	$4\pi\lambda$	$5.821\theta^{1/3}$	$2.389\theta^{1/3}\frac{24\pi^2}{35}$

Table 1: Ratio Surface area / Volume of various random grains

Similarly, Poisson strata with thickness l are obtained as a limiting case of a Boolean model of cylinders for $r \to \infty$ and an intensity $\theta \to 0$ ([8], p. 224). For this model, we get:

$$\frac{S}{V} = \lim_{l\to\infty} \frac{2(r+l)}{rl} = \frac{2}{l}$$

The size effect on L^*_{V123} is increasing from Poisson strata or fibers, to spheres and cubes.

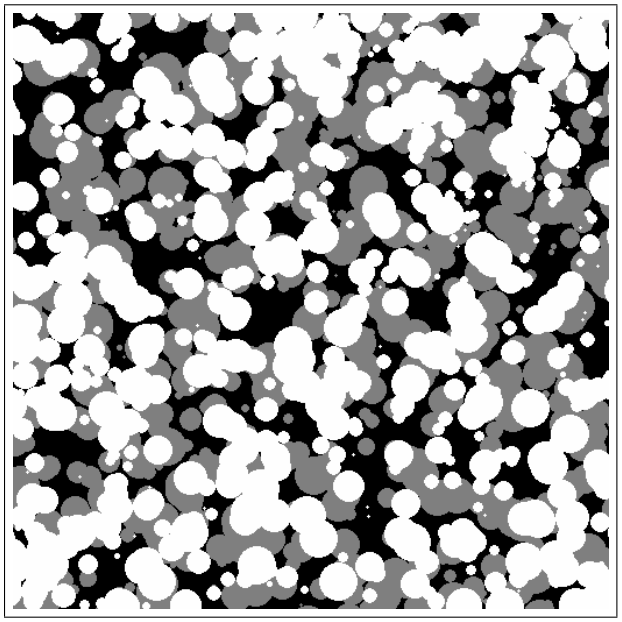

Figure 5: Superposition of two-components Boolean models with spherical primary grains ($P_1 = 0.497$, $P_2 = 0.274$, $P_3 = 0.229$)

6.2 Superposition of two-components mosaics

Consider now as primary random sets two binary mosaics (Figure 6), built on random tessellations with random cells C_1 and C_2 and with volume fractions P'_1 and P'_2. Introducing the specific surface areas given by equation (5) into

equation (24), we obtain

$$L^*_{V123} = \frac{\pi}{4} P_1(1-P_1)P'_2(1-P'_2)\frac{\overline{S}(C_1)}{\overline{V}(C_1)}\frac{\overline{S}(C_2)}{\overline{V}(C_2)} \tag{27}$$

The volume fractions maximizing L_{V123} are given by

$$P_1 = \frac{1}{2},\ P'_2 = \frac{1}{2},\ P_2 = \frac{1}{4},\ P_3 = \frac{1}{4}$$

The same size effect as for the superposition of Boolean models (subsection 6.1) is observed for this three-components model.

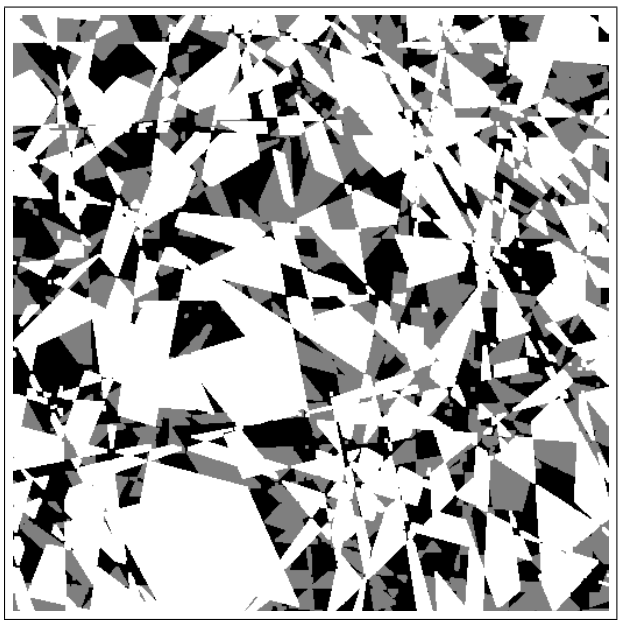

Figure 6: Superposition of two-components Poisson mosaics ($P_1 = 0.504$, $P_2 = 0.281$, $P_3 = 0.215$)

6.3 Superposition of Color Dead Leaves models

We consider random sets built from two Color Dead Leaves (Figure 7) as basic random sets A'_1 and A'_2. Each one is built from two types of grains (one for A'_i and one for ${A'_i}^c$). We have

$$C_{ii^c}(h) = P_i P_j \frac{2 - r_i(h) - r_j(h)}{2 - r(h)}$$

with

$$r(h) = \frac{\sum\limits_i \theta_i K_i(h)}{\sum\limits_i \theta_i K_i(0)} = \sum_i P_i r_i(h)$$

In the case of two components Color Dead Leaves ([8], p. 358),

$$C_{12}(h) = P_1(1-P_1)\frac{2-r_1(h)-r_2(h)}{2-r(h)}$$

and

$$C'_{12}(h) = P_1(1-P_1)\frac{(2-r(h))(-r'_1(h)-r'_2(h))+(2-r_1(h)-r_2(h))r'(h)}{(2-r(h))^2}$$

$$(C'_{12}(0))' = -P_1(1-P_1)(r'_1(0)+r'_2(0))$$

Therefore, for the combination of two Color Dead Leaves models, with primary grains A'_{11}, A'_{12}, A'_{21}, A'_{22}

$$\begin{aligned} & L^*_{V123} \\ = \; & \frac{\pi}{4}P_1(1-P_1)\left(\frac{\overline{S}(A'_{11})}{\overline{V}(A'_{11})}+\frac{\overline{S}(A'_{12})}{\overline{V}(A'_{12})}\right)P'_2(1-P'_2)\left(\frac{\overline{S}(A'_{21})}{\overline{V}(A'_{21})}+\frac{\overline{S}(A'_{22})}{\overline{V}(A'_{22})}\right) \end{aligned} \tag{28}$$

It is easy to deduce that the volume fractions maximizing L_{V123} are given by

$$P_1 = \frac{1}{2},\; P'_2 = \frac{1}{2},\; P_2 = \frac{1}{4},\; P_3 = \frac{1}{4}$$

For these volume fractions, equation (28) becomes

$$L^*_{V123\max} = \frac{\pi}{64}\left(\frac{\overline{S}(A'_{11})}{\overline{V}(A'_{11})}+\frac{\overline{S}(A'_{12})}{\overline{V}(A'_{12})}\right)\left(\frac{\overline{S}(A'_{21})}{\overline{V}(A'_{21})}+\frac{\overline{S}(A'_{22})}{\overline{V}(A'_{22})}\right)$$

The same conclusion as for the superposition of Boolean models can be derived about the decrease of L_{V123} with the size of primary grains. When using only two types of primary grains, $A'_{11} = A'_{12} = A'_1$ and $A'_{21} = A'_{22} = A'_2$, it comes

$$L^*_{V123\max} = \frac{\pi}{16}\frac{\overline{S}(A'_1)}{\overline{V}(A'_1)}\frac{\overline{S}(A'_2)}{\overline{V}(A'_2)} \simeq 0.1963\frac{\overline{S}(A'_1)}{\overline{V}(A'_1)}\frac{\overline{S}(A'_2)}{\overline{V}(A'_2)}$$

so that the superposition of two Color Dead Leaves random sets provides a triple boundary line with length about two times more than what is obtained for the Boolean model with the same grains and optimal volume fractions. It is also instructive to compare this result to the three Color Dead Leaves, for which the maximized length is given by:

$$L^*_{V123\max} = \frac{\pi}{18}\left(\frac{\overline{S}(A')}{\overline{V}(A')}\right)^2 \simeq 0.17453\left(\frac{\overline{S}(A')}{\overline{V}(A')}\right)^2$$

which is close to the result obtained for the superposition of two Color Dead Leaves random sets with optimal volume fraction. Dead Leaves models provide more fragmented textures than Boolean models with the same primary grains, providing microstructures with longer triple lines, up to a factor close to two.

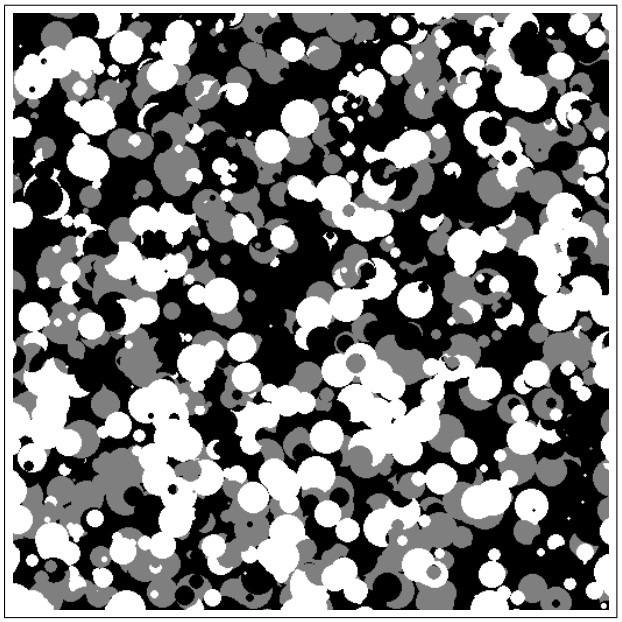

Figure 7: Superposition of two-components Color Dead Leaves with spherical primary grains
($P_1 = 0.336$, $P_2 = 0.239$, $P_3 = 0.425$)

6.4 Superposition of random sets generated by dilution random functions

Consider a random function model given by the random number $N(x)$ of primary grain A' covering x, grains being located on points of a Poisson point process with intensity θ ([8], p. 542). It is a variant of the Dilution random function. The set obtained with zero grain is the complementary set of a Boolean model with primary grain A' and covariance $Q(h)$ with derivative

$$Q'(0) = \frac{d}{dh}\left(\exp(-\theta K(0)(2 - r(h)))\right)_{h=0} = -q \log q r'(0)$$

The random number N of grains hitting x is a Poisson random variable with intensity $a = \theta K(0)$, and with probability P_n. The set A_n where $N(x) = n$ has for volume fraction:

$$P_n = \frac{a^n}{n!} \exp(-a) = \frac{a^n}{n!} q$$

We have

$$P_{n+1} - P_n = q\left(\frac{a^{n+1}}{(n+1)!} - \frac{a^n}{n!}\right) = q\frac{a^n}{n!}(\frac{a}{n+1} - 1)$$

so that $P_{n+1} < P_n$ for $a < n+1$. Therefore P_n is decreasing with n for n large enough, and for a given a, $P_n \to 0$ when $n \to \infty$.

For a given $n > 0$, a maximal volume fraction can be reached. We have

$$\frac{d}{da}P_n = \frac{a^{n-1}}{(n-1)!}\exp(-a) - \frac{a^n}{(n)!}\exp(-a) = \frac{a^{n-1}}{(n-1)!}\exp(-a)(1 - \frac{a}{n})$$

and the maximum of P_n is given for $a = n$. We get:

n	1	2	3	4	5
$q = \exp(-n)$	0.367 88	0.135 34	0.0498	0.01 83	0.00673
$\frac{n^n}{n!}\exp(-n)$	0.367 88	0.270 67	0.224 04	0.195 37	0.175 47

6	7	8	9	10
0.002 5	9×10^{-4}	3.35×10^{-4}	1.2×10^{-4}	4.5×10^{-5}
0.160 62	0.149	0.139 59	0.131 76	0.125 11

The morphology of the sets A_n is very specific: by construction, A_n is very fragmented, and there is no contact between sets A_n and A_{n+k} for $k > 1$, and between sets A_n and A_{n-k} for $k > 1$. Contacts occur only between components A_n, A_{n-1} and A_{n+1}. We will denote by $C_n(h)$ the covariance of the set A_n.

For illustration, we consider cases with $n = 1, 2, 3, 4, ...n$. The covariances of sets A_1, A_2, A_3, A_4 are given by ([8], p. 545-546):

$$\begin{aligned}
C_1(h) &= Q(h)a(a(1-r(h))^2 + r(h)) \\
C_2(h) &= Q(h)\frac{a^2}{4}(a^2(1-r(h))^4 + 4ar(h)(1-r(h))^2 + 2r(h)^2) \\
C_3(h) &= Q(h)\frac{a^3}{3!3!}(a^3(1-r(h))^6 + 9a^2r(h)(1-r(h))^4 + 18ar(h)^2(1-r(h))^2 + 6r(h)^3) \\
C_4(h) &= Q(h)\frac{a^4}{4!4!}\left(a^4(1-r(h))^8 + 16a^3r(h)(1-r(h))^6\right. \\
&\quad \left. +72a^2r(h)^2(1-r(h))^4 + 96ar(h)^3(1-r(h))^2 + 24r(h)^4\right)
\end{aligned}$$

where $r(h) = \frac{K(h)}{K(0)}$ and $a = \theta K(0) = -\log q$. The specific surface areas of sets A_1, A_2, A_3, A_4, are obtained from the derivative of the covariance in $h = 0$.

6.4.1 Random set A_1

A realization of a 2D section of a 3D model obtained by superposition of two random sets A_1 is shown on Figure 8.

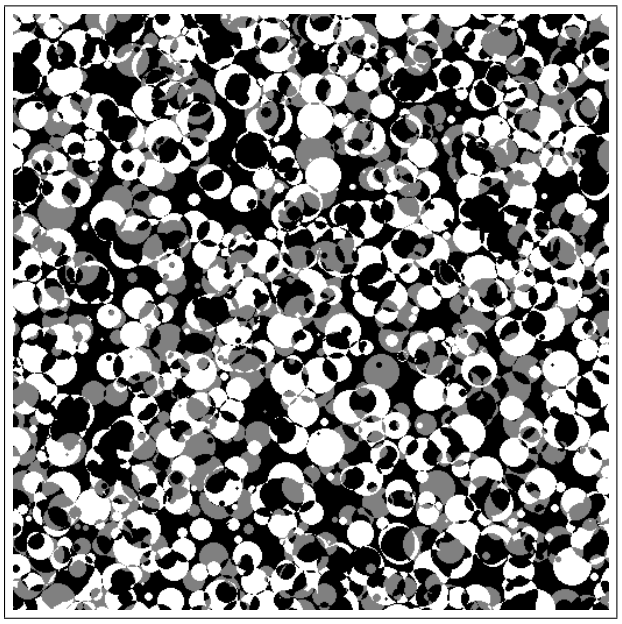

Figure 8: Superposition of two-components level sets ($N(x) = 1$) of Dilution RF with spherical primary grains ($P_1 = 0.376$, $P_2 = 0.200$, $P_3 = 0.424$)

The derivative of the covariance $C_1(h)$ is given by:

$$\begin{aligned} C_1'(0) &= Q'(0)a + Q(0)ar'(0) = a(-r'(0)q\log q + qr'(0)) = ar'(0)q(-\log q + 1) \\ &= -q\log qr'(0)(1-\log q) \end{aligned}$$

and

$$S_{V_1} = -\frac{\overline{S}(A')}{\overline{V}(A')} q\log q(1-\log q) = \frac{\overline{S}(A')}{\overline{V}(A')} qa(1+a)$$

giving

$$L^*_{V_{123}} = \frac{\pi}{4}\left(\frac{\overline{S}(A')}{\overline{V}(A')}\right)^2 q^2a^2(1+a)^2 \tag{29}$$

For a given primary grain, the maximum of S_{V_1} is obtained for

$$\begin{aligned} \frac{d}{dq}\left(q\log q(1-\log q)\right) &= -\frac{1}{q}q\log q + (1-\log q)(1+\log q) \\ &= -\log q + (1-\log q)(1+\log q) \\ &= -\log q + 1 - (\log q)^2 = 0 \text{ for } q = e^{-\frac{1}{2}\sqrt{5}-\frac{1}{2}} = 0.198\,29 \end{aligned}$$

$$1 + a - a^2 = 0,\ a = \frac{1+\sqrt{5}}{2}$$

and

$$q = \exp(-\frac{1+\sqrt{5}}{2}) = 0.198\,29$$

for which

$$\begin{aligned} S_{V_1\,\max} &= -\frac{\overline{S}(A')}{\overline{V}(A')} 0.198\,29(1 - \log 0.198\,29)\log(0.198\,29) \\ &= \frac{\overline{S}(A')}{\overline{V}(A')} 0.839\,96 \end{aligned}$$

giving

$$L^*_{V_{123}\,\max} = \frac{\pi}{4} \times 0.839\,96^2 \left(\frac{\overline{S}(A')}{\overline{V}(A')}\right)^2 = 0.554\,12 \left(\frac{\overline{S}(A')}{\overline{V}(A')}\right)^2$$

so that $L^*_{V_{123}}$ obtained for that model is about five times the maximal value obtained for the Boolean model with the same grains ($\frac{\pi}{4}\exp -2$), and about three times the maximal value of the Color Dead Leaves model with the same gains.

The maximum of S_{V_1} is obtained for

$$P_1 = -0.198\,29 \log 0.198\,29 = 0.320\,84$$

6.4.2 Random set A_2

A realization of a 2D section of a 3D model obtained by superposition of two random sets A_2 is shown on Figure 9. The derivative of the covariance $C_2(h)$ is given by:

$$C_2'(0) = Q'(0)\frac{a^2}{2} + q\frac{a^2}{4}4r'(0)$$

and

$$S_{V_2} = \frac{\overline{S}(A')}{\overline{V}(A')}\left(\frac{a^2}{2}qa + qa^2\right) = \frac{\overline{S}(A')}{\overline{V}(A')}qa^2(\frac{a}{2}+1)$$

giving

$$L^*_{V_{123}} = \frac{\pi}{4}\left(\frac{\overline{S}(A')}{\overline{V}(A')}\right)^2 q^2a^4(\frac{a}{2}+1)^2 \qquad (30)$$

the maximum of S_{V_2} is obtained for

$$\begin{aligned}
\frac{d}{dq}\left(qa^2(\frac{a}{2}+1)\right) &= 0 \\
-\frac{1}{2}qa^2\frac{1}{q}+(\frac{a}{2}+1)(a^2-2a) &= 0 \\
-\frac{a}{2}+(\frac{a}{2}+1)(a-2) &= 0 \\
-a+(a+2)(a-2) &= 0 \\
a^2-a-4 &= 0
\end{aligned}$$

$$a^2-a-4=0,\ a=\frac{1+\sqrt{17}}{2}$$

and

$$q=\exp(-\frac{1+\sqrt{17}}{2})=7.718\,5\times10^{-2}$$

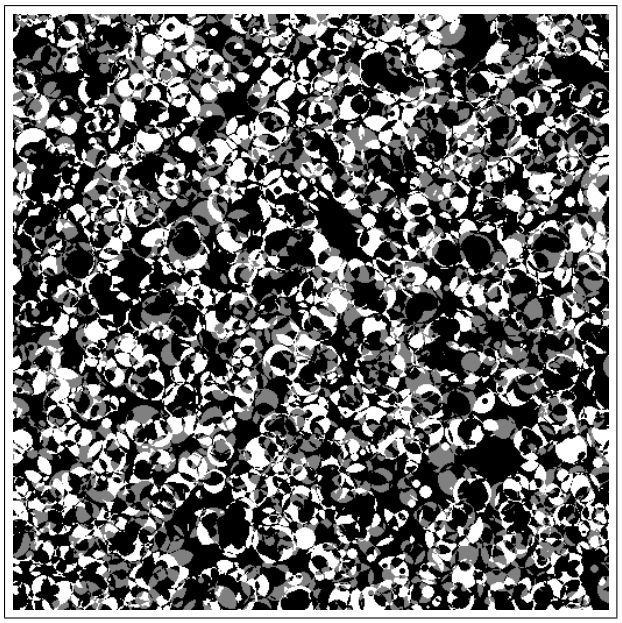

Figure 9: Superposition of two-components level sets ($N(x)=2$) of Dilution RF with spherical primary grains ($P_1=0.283$, $P_2=0.194$, $P_3=0.523$)

for which

$$\begin{aligned}
S_{V_2\max} &= -\frac{\overline{S}(A')}{\overline{V}(A')}7.718\,5\times10^{-2}(\log 7.718\,5\times10^{-2})^2(1+\frac{\log 7.718\,5\times10^{-2}}{2}) \\
&= \frac{\overline{S}(A')}{\overline{V}(A')}1.155\,1
\end{aligned}$$

giving

$$L^*_{V_{123}\,\max} == \frac{\pi}{4} 1.155\,1^2 \left(\frac{\overline{S}(A')}{\overline{V}(A')}\right)^2 = 1.047\,9 \left(\frac{\overline{S}(A')}{\overline{V}(A')}\right)^2$$

providing a triple boundary length about 10 times higher than for the Boolean model with the same grains. The maximum of S_{V_2} is obtained for

$$P_2 = \left(\frac{1+\sqrt{17}}{2}\right)^2 \frac{1}{2} \exp(-\frac{1+\sqrt{17}}{2}) = 0.253\,23$$

6.4.3 Random set A_3

A realization of a 2D section of a 3D model obtained by superposition of two random sets A_3 is shown on Figure 10.

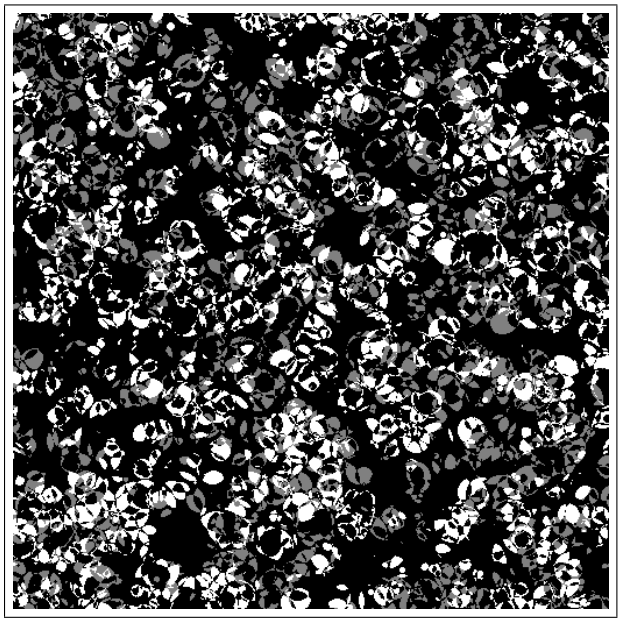

Figure 10: Superposition of two-components level sets ($N(x) = 3$) of Dilution RF with spherical primary grains ($P_1 = 0.19$, $P_2 = 0.145$, $P_3 = 0.665$)

The derivative of the covariance $C_3(h)$ is given by:

$$\begin{aligned} C_3'(0) &= Q'(0)\frac{a^3}{3!3!}6 + q\frac{a^3}{3!3!}18r'(0) \\ &= a^3(\frac{Q'(0)}{6} + \frac{q}{2}r'(0)) \end{aligned}$$

and

$$S_{V_3} = \frac{a^3}{3!} q \frac{\overline{S}(A')}{\overline{V}(A')} (a+3)$$

giving

$$L^*_{V_{123}} = \frac{\pi}{4} \left(\frac{\overline{S}(A')}{\overline{V}(A')} \right)^2 \left(\frac{a^3}{3!} q (a+3) \right)^2 \tag{31}$$

the maximum of S_{V_3} is obtained for

$$\frac{d}{dq} \left(a^3 \left(\frac{q}{6} a + \frac{q}{2} \right) \right) = 0$$

$$\begin{aligned}
-\frac{1}{q} 3a^2 \left(\frac{q}{6} a + \frac{q}{2} \right) + a^3 (\frac{a}{6} - \frac{1}{6} + \frac{1}{2}) &= 0 \\
-3a^2 \left(\frac{1}{6} a + \frac{1}{2} \right) + a^3 (\frac{a}{6} + \frac{1}{3}) &= 0 \\
\left(-\frac{1}{2} a - \frac{3}{2} \right) + a (\frac{1}{3} + \frac{a}{6}) &= 0 \\
-9 - 3a + a(2+a) &= 0 \\
-9 - a + a^2 &= 0 \\
a^2 - a - 9 &= 0
\end{aligned}$$

$$a^2 - a - 9 = 0,\ a = \frac{1+\sqrt{37}}{2}$$

and

$$q = \exp(-\frac{1+\sqrt{37}}{2}) = 2.897\,3 \times 10^{-2}$$

for which

$$\begin{aligned}
S_{V_3 \max} &= -\frac{\overline{S}(A')}{\overline{V}(A')} 2.897\,3 \times 10^{-2} (\frac{1+\sqrt{37}}{2})^3 (\frac{1}{2} + \frac{1+\sqrt{37}}{12}) \\
&= \frac{\overline{S}(A')}{\overline{V}(A')} 1.402\,9
\end{aligned}$$

giving

$$L^*_{V_{123}\max} = \frac{\pi}{4} 1.402\,9^2 \left(\frac{\overline{S}(A')}{\overline{V}(A')} \right)^2 = 1.545\,8 \left(\frac{\overline{S}(A')}{\overline{V}(A')} \right)^2$$

providing a triple boundary length about 14 times higher than for the Boolean model with the same grains. The maximum of S_{V_3} is obtained for

$$P_3 = \frac{1}{6} \left(\frac{1+\sqrt{37}}{2} \right)^3 \exp(-\frac{1+\sqrt{37}}{2}) = 0.214\,47$$

6.4.4 Random set A_4

The derivative of the covariance $C_4(h)$ is given by:

$$\begin{aligned} C_4'(0) &= Q'(0)\frac{24a^4}{4!4!} + q\frac{24a^4}{4!4!}4r'(0) \\ &= q\frac{24a^4}{4!4!}\left(ar'(0) + 4r'(0)\right) \\ &= q\frac{24a^4}{4!4!}r'(0)(a+4) \end{aligned}$$

$$S_{V_4} = \frac{\overline{S}(A')}{\overline{V}(A')}q\frac{24a^4}{4!4!}(a+4) = \frac{\overline{S}(A')}{\overline{V}(A')}q\frac{a^4}{4!}(a+4)$$

giving

$$L^*_{V_{123}} = \frac{\pi}{4}\left(\frac{\overline{S}(A')}{\overline{V}(A')}\right)^2\left(q\frac{a^4}{4!}(a+4)\right)^2 \tag{32}$$

the maximum of S_{V_4} is obtained for

$$\begin{aligned} \frac{d}{dq}S_{V_4} &= 0 \text{ for} \\ -qa^4\frac{1}{q} + (a+4)(a^4-4a^3) &= 0 \\ -a + (a-4)(a+4) &= 0 \\ a^2 - a - 16 &= 0,\ a = \frac{1+\sqrt{65}}{2} \end{aligned}$$

and

$$q = \exp(-\frac{1+\sqrt{65}}{2}) = 1.076\,9 \times 10^{-2}$$

for which

$$\begin{aligned} S_{V_4\max} &= -\frac{\overline{S}(A')}{\overline{V}(A')}1.076\,9 \times 10^{-2}(\frac{1+\sqrt{65}}{2})^4(4+\frac{1+\sqrt{65}}{2})\frac{1}{24} \\ &= \frac{\overline{S}(A')}{\overline{V}(A')}1.613\,6 \end{aligned}$$

giving

$$L^*_{V_{123}\max} = \frac{\pi}{4}1.613\,6^2\left(\frac{\overline{S}(A')}{\overline{V}(A')}\right)^2 = 2.044\,9\left(\frac{\overline{S}(A')}{\overline{V}(A')}\right)^2$$

providing a triple boundary length about 19 times higher than for the Boolean model with the same grains. The maximum of S_{V_4} is obtained for

$$P_4 = \frac{1}{4!}\left(\frac{1+\sqrt{65}}{2}\right)^4 \exp(-\frac{1+\sqrt{65}}{2}) = 0.189\,13$$

6.4.5 Random set A_n

More generally, for any n; S_{V_n} is obtained by induction:

$$S_{V_n} = \frac{\overline{S}(A')}{\overline{V}(A')} q \frac{a^n}{n!}(a+n) \tag{33}$$

For a fixed, S_{V_n} decreases with n, for n large enough:

$$\begin{aligned} S_{V_{n+1}} - S_{V_n} &= \frac{\overline{S}(A')}{\overline{V}(A')} q \left(\frac{a^{n+1}}{(n+1)!}(a+n+1) - \frac{a^n}{n!}(a+n)\right) \\ &= \frac{\overline{S}(A')}{\overline{V}(A')} q \frac{a^n}{n!}\left(\frac{a}{n+1}(a+n+1) - (a+n)\right) \\ &= \frac{\overline{S}(A')}{\overline{V}(A')} q \frac{a^n}{n!}\frac{1}{n+1}\left(a^2 - n^2 - n\right) \end{aligned}$$

and $S_{V_{n+1}} < S_{V_n}$ when $a^2 - n^2 - n < 0$, or $n^2 + n > a^2$. Therefore, for fixed a, $S_{V_n} \to 0$ when $n \to \infty$. We have

$$L^*_{V_{123}} = \frac{\pi}{4}\left(\frac{\overline{S}(A')}{\overline{V}(A')}\right)^2 q^2 \frac{a^{2n}}{n!n!}(a+n)^2 \tag{34}$$

For n given, S_{V_n} reaches a maximum obtained from

$$\frac{d}{dq} S_{V_n} = \frac{\overline{S}(A')}{\overline{V}(A')}\left(\frac{a^n}{n!}(a+n) - \frac{a^n}{n!} - \frac{a^{n-1}}{(n-1!}(a+n)\right)$$

$\frac{d}{dq} S_{V_n} = 0$ for

$$\begin{aligned} \frac{a}{n}(a+n) - \frac{a}{n} - a - n &= 0 \\ \frac{a^2}{n} + a - \frac{a}{n} - a - n &= 0 \\ a^2 - a - n^2 &= 0,\ a = \frac{1+\sqrt{n^2+1}}{2} \end{aligned}$$

for which

$$S_{V_n\max} = \frac{\overline{S}(A')}{\overline{V}(A')}\exp - \left(\frac{1+\sqrt{n^2+1}}{2}\right)\frac{\left(\frac{1+\sqrt{n^2+1}}{2}\right)^n}{n!}(\frac{1+\sqrt{n^2+1}}{2}+n)$$

and

$$L^*_{V_{123}\max} = \frac{\pi}{4}\left(\frac{\overline{S}(A')}{\overline{V}(A')}\right)^2\exp - \left(1+\sqrt{n^2+1}\right)\frac{\left(\frac{1+\sqrt{n^2+1}}{2}\right)^{2n}}{n!n!}\left(\frac{1+\sqrt{n^2+1}}{2}+n\right)^2$$

This maximal value is obtained for the volume fraction

$$P_n = \exp - \left(\frac{1+\sqrt{n^2+1}}{2}\right)\frac{\left(\frac{1+\sqrt{n^2+1}}{2}\right)^n}{n!}$$

6.5 Superposition of excursion random sets of dilution random functions

Consider now the excursion random sets of $N(x)$. By definition,

$$A_N(m) = \{x, N(x) \geq m\}$$

It can be viewed as a Boolean model with primary grain A', from which are progressively removed grains, starting from $A_N(m)^c$. The volume fraction of $A_N(m)$ is given by

$$P_m = 1 - \sum_{k=0}^{k=m-1}\frac{a^k}{k!}\exp(-a) = 1 - q\sum_{k=0}^{k=m-1}\frac{a^k}{k!}$$

The set obtained for $m = 1$ is the Boolean model with primary grain A' and with covariance

$$Q_1(h) = Q(h) = \exp\left(-\theta K(0)(2 - r(h))\right)$$

The covariance of the complementary set of $A_N(m)$ is given by

$$Q_m(h) = P\left\{N(x) < m, N(x+h)\right\} < m$$

By construction,

$$A_N(m+1)^c = A_N(m)^c \cup A_m$$

and

$$Q_{m+1}(h) = Q_m(h) + C_m(h) + 2\sum_{k<m} P\left\{N(x) = m, N(x+h) = k\right\}$$

To estimate the specific surface area of the set $A_N(m+1)$, we have to compute the derivative $Q'_{m+1}(0)$. Since there is no contact between A_m and A_{m-k} for $k > 1$ it comes

$$Q'_{m+1}(0) = Q'_m(0) + C'_m(0) + 2\frac{\partial}{\partial h}\left(P\left\{N(x) = m, N(x+h) = m-1\right\}\right)_{h=0}$$

The covariances can be useful to fit the parameters of a model. For $m = 2, 3, 4$, we have ([8], p. 548):

$$\begin{aligned}
Q_2(h) &= Q(h)\left(a^2(1-r(h))^2 + a(2-r(h)) + 1\right) \\
Q_3(h) &= Q(h)\left(\frac{a^4(1-r(h))^4}{4} + a^3(1-r(h))^2 + \frac{a^2(2-r(h))^2}{2} + a(2-r(h)) + 1\right) \\
Q_4(h) &= Q(h)\left(\frac{a^2}{2}(2-r(h))^2 + \frac{a^3}{6}(2-r(h))^3 + \frac{a^6}{36}(1-r(h))^6 + a(2-r(h)\right. \\
&\quad \left. + \frac{a^4}{12}(1-r(h))^2(r(h)^2 - 2r(h) + 7) + \frac{a^5}{12}(1-r(h))^4(r(h)+2) + 1\right)
\end{aligned}$$

6.5.1 Random set $A_N(2)$

From the definition of $A_N(m)$ we have for $m = 2$

$$\begin{aligned}
Q_2(h) &= Q(h) + C_1(h) + 2P\left\{N(x) = 0, N(x+h) = 1\right\} \\
&= Q(h) + C_1(h) + 2aQ(h)(1-r(h))
\end{aligned}$$

and

$$\begin{aligned}
Q'_2(0) &= Q'(0) + C'_1(0) - 2qar'(0) = qar'(0) + qar'(0)(1+a) - 2qar'(0) \\
&= qar'(0)(1 + (1+a) - 2) = qa^2r'(0)
\end{aligned}$$

The specific surface area of $A_N(2)$ is given by

$$S_V(2) = \frac{\overline{S}(A')}{\overline{V}(A')}qa^2$$

and

$$L^*_{V_{123}} = \frac{\pi}{4}\left(\frac{\overline{S}(A')}{\overline{V}(A')}\right)^2 q^2a^4 \tag{35}$$

$S_V(2)$ is maximal for

$$a^2 - 2a = 0,\ a = 2$$

$$S_{V_{\max}}(2) = \frac{\overline{S}(A')}{\overline{V}(A')} 4 \exp -2 = 0.541\,34 \frac{\overline{S}(A')}{\overline{V}(A')}$$

giving

$$L^*_{V_{123}\,\max} = \frac{\pi}{4} 0.541\,34^2 \left(\frac{\overline{S}(A')}{\overline{V}(A')} \right)^2 = 0.230 \left(\frac{\overline{S}(A')}{\overline{V}(A')} \right)^2$$

providing a triple boundary length about 2 times higher than for the Boolean model with the same grains. It is reached for the volume fraction

$$P = 1 - (1+2) \exp -2 = 0.593\,99$$

6.5.2 Random set $A_N(3)$

We have

$$\begin{aligned} Q_3(h) &= Q_2(h) + C_2(h) + 2P\{N(x) = 2, N(x+h) = 0\} + 2P\{N(x) = 2, N(x+h) = 1\} \\ &= Q_2(h) + C_2(h) + Q(h)a^2(1 - r(h))(a(1 - r(h))^2 + 2r(h)) + a^2 Q(h)(1 - r(h))^2 \end{aligned}$$

and

$$\begin{aligned} Q_3'(0) &= Q_2'(0) + C_2'(0) - 2r'(0)qa^2 = qa^2 r'(0) + qa^2 r'(0)(\frac{a}{2} + 1) - 2r'(0)qa^2 \\ &= qr'(0)\frac{a^3}{2} \end{aligned}$$

so that the specific surface area of $A_N(3)$ is given by

$$S_V(3) = \frac{\overline{S}(A')}{\overline{V}(A')} q \frac{a^3}{2}$$

and

$$L^*_{V_{123}} = \frac{\pi}{4} \left(\frac{\overline{S}(A')}{\overline{V}(A')} \right)^2 q^2 \frac{a^6}{4} \tag{36}$$

$S_V(3)$ is maximal for

$$\frac{a^3}{2} - \frac{3}{2}a^2 = 0,\ a = 3$$

the maximal surface area is given by

$$S_{V_{\max}}(3) = \frac{\overline{S}(A')}{\overline{V}(A')} \frac{27}{2} \exp(-3) = 0.672\,13 \frac{\overline{S}(A')}{\overline{V}(A')}$$

and

$$L^*_{V_{123}\max} = \frac{\pi}{4} 0.672\,13^2 \left(\frac{\overline{S}(A')}{\overline{V}(A')}\right)^2 = 0.354\,8 \left(\frac{\overline{S}(A')}{\overline{V}(A')}\right)^2$$

providing a triple boundary length about 3 times higher than for the Boolean model with the same grains. It is reached for the volume fraction

$$P = 1 - (1 + 3 + \frac{9}{2}) \exp -3 = 0.576\,81$$

6.5.3 Random set $A_N(4)$

We have

$$Q'_4(0) = Q'_3(0) + C'_3(0) + 2\frac{\partial}{\partial h} \left(P\left\{N(x) = 3, N(x+h) = 2\right\}\right)_{h=0}$$

with

$$\begin{aligned} & P\left\{N(x) = 3, N(x+h) = 2\right\} \\ = \; & \frac{a^3}{12} Q(h) \left(1 - r(h))a^2 r(h)^4 - 4a^2 r(h)^3 + 6a^2 r(h)^2 - 4a^2 r(h) + a^2 \right. \\ & \left. +6ar(h)^3 - 12ar(h)^2 + 6ar(h) + 6r(h)^2\right) \end{aligned}$$

and

$$2\frac{\partial}{\partial h} \left(P\left\{N(x) = 3, N(x+h) = 2\right\}\right)_{h=0} = -qa^3 r'(0)$$

$$\begin{aligned} Q'_4(0) &= qr'(0)\frac{a^3}{2} + a^3\left(\frac{aqr'(0)}{6} + \frac{q}{2} r'(0)\right) - qa^3 r'(0) \\ &= qr'(0)\frac{a^4}{6} \end{aligned}$$

so that the specific surface area of $A_N(4)$ is given by

$$S_V(4) = \frac{\overline{S}(A')}{\overline{V}(A')} q \frac{a^4}{3!}$$

and

$$L^*_{V_{123}} = \frac{\pi}{4} \left(\frac{\overline{S}(A')}{\overline{V}(A')}\right)^2 q^2 \frac{a^8}{3!3!} \tag{37}$$

which is maximal for

$$a^4 - 4a^3 = 0,\; a = 4$$

the maximal surface area is given by

$$S_{V_{\max}}(4) = \frac{\overline{S}(A')}{\overline{V}(A')}\frac{4^4}{3!}\exp(-4) = 0.781\,47\frac{\overline{S}(A')}{\overline{V}(A')}$$

$$L^*_{V_{123}\max} = \frac{\pi}{4}0.781\,47^2\left(\frac{\overline{S}(A')}{\overline{V}(A')}\right)^2 = 0.479\,64\left(\frac{\overline{S}(A')}{\overline{V}(A')}\right)^2$$

providing a triple boundary length about 4.5 times higher than for the Boolean model with the same grains. It is reached for the volume fraction

$$P = 1 - (1 + 4 + \frac{16}{2} + \frac{64}{6})\exp -4 = 0.566\,53$$

6.5.4 Random set $A_N(m)$

More generally it is interesting to consider the random set $A_N(m)$. A realization of a 2D section of a 3D model obtained by superposition of two random sets $A_N(5)$ is shown on Figure 11.

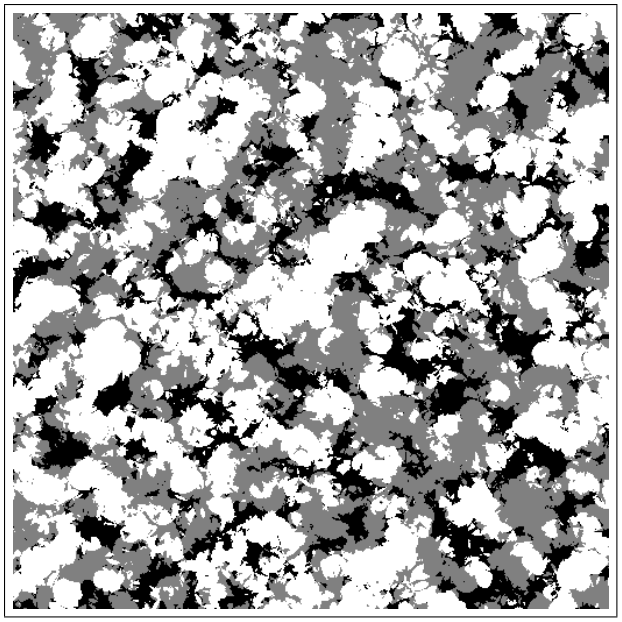

Figure 11: Superposition of two-components thresholded (≥ 5) Dilution RF with spherical primary grains
($P_1 = 0.456$, $P_2 = 0.347$, $P_3 = 0.197$)

We can infer that the specific surface area of $A_N(m)$ is given by

$$S_V(m) = \frac{\overline{S}(A')}{\overline{V}(A')}q\frac{a^m}{(m-1)!} \tag{38}$$

and

$$L^*_{V_{123}} = \frac{\pi}{4}\left(\frac{\overline{S}(A')}{\overline{V}(A')}\right)^2 q^2 \frac{a^{2m}}{(m-1)!(m-1)!} \tag{39}$$

We have

$$S_V(m+1) - S_V(m) = \frac{\overline{S}(A')}{\overline{V}(A')} q \frac{a^m}{(m-1)!}\left(\frac{a}{m} - 1\right)$$

and $S_V(m+1) > S_V(m)$ for $a > m$. When this condition is fulfilled, $S_V(m)$ grows with m. $S_V(m)$ is maximal for $a = m$. We have:

$$S_{V_{\max}}(m) = \frac{\overline{S}(A')}{\overline{V}(A')} \frac{m^m}{(m-1)!} \exp(-m)$$

$$\begin{aligned}
S_{V_{\max}}(m) - S_{V_{\max}}(m-1) &= \frac{\overline{S}(A')}{\overline{V}(A')}\left(\frac{m^m}{(m-1)!}\exp(-m) - \frac{(m-1)^{m-1}}{(m-2)!}\exp(-(m-1)\right) \\
&= \frac{\overline{S}(A')}{\overline{V}(A')}\frac{\exp(-(m-1)}{(m-2)!}\left(\frac{m^m}{(m-1)}e - (m-1)^{m-1}\right) \\
&= \frac{\overline{S}(A')}{\overline{V}(A')}\frac{\exp(-(m-1)(m-1)^{m-1}}{(m-2)!}\left(\frac{m^m}{(m-1)(m-1)^{m-1}}e - 1\right) \\
&= \frac{\overline{S}(A')}{\overline{V}(A')}\frac{\exp(-(m-1)(m-1)^{m-1}}{(m-2)!}\left(\frac{m^m}{(m-1)^m}e - 1\right)
\end{aligned}$$

and therefore

$$S_{V_{\max}}(m) > S_{V_{\max}}(m-1)$$

The maximal surface area is growing with m. We have:

$$L^*_{V_{123}\,\max} = \frac{\pi}{4}\left(\frac{\overline{S}(A')}{\overline{V}(A')}\right)^2 \frac{m^{2m}}{(m-1)!(m-1)!}\exp(-2m)$$

6.6 Superposition of random sets generated by two thresholds of dilution random functions

Consider now the random set $A_N(m,n)$ defined for $n > m$ by

$$A_N(m,n) = \{x, m \leq N(x) < n\}$$

A realization of a 2D section of a 3D model obtained by superposition of two random sets $A_N(10,15)$ is shown on Figure 12.

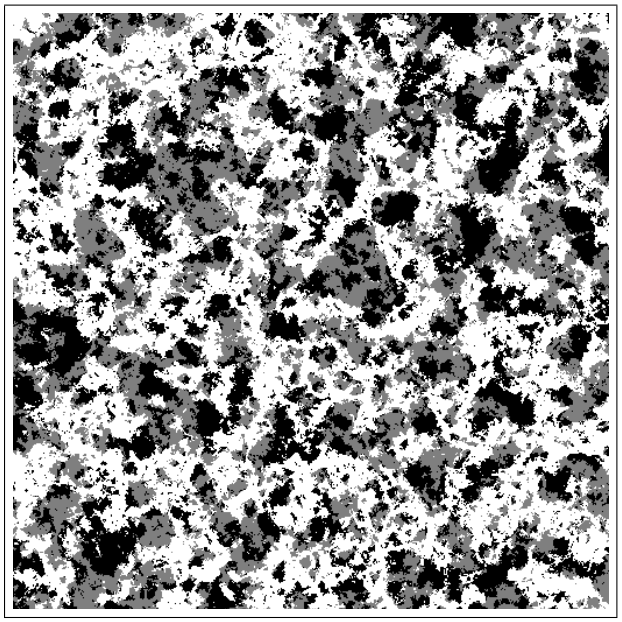

Figure 12: Superposition of two-components thresholded ($10 \leq Z(x) \leq 15$)
Dilution RF with spherical primary grains
($P_1 = 0.435$, $P_2 = 0.264$, $P_3 = 0.301$)

From the definition of $A_N(m,n)$, we have

$$A_N(m,n) = A_N(m) \cap A_N(n)^c$$

and therefore

$$A_N(m,n)^c = A_N(m)^c \cup A_N(n)$$

The covariance $Q_{mn}(h)$ of set $A_N(m,n)^c$ is given by

$$Q_{mn}(h) = Q_m(h) + Cov_{A_N(n)}(h) + 2Cov_{A_N(n),A_N(m)^c}(h)$$

where $Cov_{A_N(n)}(h)$ is the covariance of $A_N(n)$ and $Cov_{A_N(n),A_N(m)^c}(h)$ the cross covariance between the two sets $A_N(n)$ and $A_N(m)^c$. Since there is no contact between these two sets, $S_{VA_N(n),A_N(m)^c} = 0$, and the specific surface area of $A_N(m,n)$ is given by

$$S_V(m,n) = S_V(m) + S_V(n)$$

and, using equation (38), we get

$$S_V(m,n) = \frac{\overline{S}(A')}{\overline{V}(A')} q \left(\frac{a^n}{(n-1)!} + \frac{a^m}{(m-1)!} \right) \tag{40}$$

When $n = m + 1$ equation (40) recovers the expression of S_{V_n} given by equation (33). Since $S_V(m)$ grows with m for $m < a$ and $S_V(n)$ grows with n when $n < a$, $S_V(m, n)$ grows with m and n (for a given $n-m$) when $n < a$.

We have

$$L^*_{V_{123}} = \frac{\pi}{4}\left(\frac{\overline{S}(A')}{\overline{V}(A')}\right)^2 q^2 \left(\frac{a^n}{(n-1)!} + \frac{a^m}{(m-1)!}\right)^2 \tag{41}$$

As before, we can look for a maximum of $S_V(m, n)$ with respect to q. From a derivation of equation (40), we have to satisfy

$$\frac{a^n}{(n-1)!} + \frac{a^m}{(m-1)!} - \left(n\frac{a^n - 1}{(n-1)!} + m\frac{a^{m-1}}{(m-1)!}\right) = 0$$

$$\frac{a^{n-m+1}}{(n-1)!} + \frac{a}{(m-1)!} - \frac{n}{(n-1)!}a^{n-m} - \frac{m}{(m-1)!} = 0$$

$$\frac{a-m}{(m-1)!} = a^{n-m}\left(\frac{n-a}{(n-1)!}\right)$$

The solution has to satisfy $a^{n-m} > 0$ and therefore $\frac{a-m}{n-a} > 0$, so that $m < a < n$. It is a root of a polynomial of degree $n - m + 1$.

6.7 Superposition of truncated Gaussian random functions

As far as we know, the use of independent truncated Gaussian RF was first introduced in [10]. It was then proposed by [1] and compared to the superposition of Boolean models. In [17] an estimation of L^*_{V123} is derived by means of equation (42). Many further studies using this model and its generalizations were published, among others [15]. This model is illustrated by Figure 13.

For random sets A'_1 and A'_2 obtained by thresholding two Gaussian random functions with correlations functions $\rho_1(h)$ and $\rho_2(h)$, the specific surface areas in equation (24) are finite when $\rho_i(h)$ are twice differentiable when $h = 0$. We get

$$S_V = -4C'(0) = \frac{2}{\pi}\exp(-\frac{\lambda^2}{2})\sqrt{-\rho''(0)}$$

This result is obtained as follows: for a truncated Gaussian RF $Z(x) \geq \lambda$ we get a random set A_λ with covariance $C(h)$. We have [9]

$$C(h) - p^2 = \frac{1}{2\pi}\int_0^{\rho(h)} \frac{\exp\left(-\frac{\lambda^2}{1+z}\right)}{\sqrt{1-z^2}}dz$$

and

$$C'(h) = \frac{1}{2\pi} \frac{\exp\left(-\frac{\lambda^2}{1+\rho(h)}\right)}{\sqrt{1-\rho^2(h)}} \rho'(h)$$

with $\rho(0) = 1$.

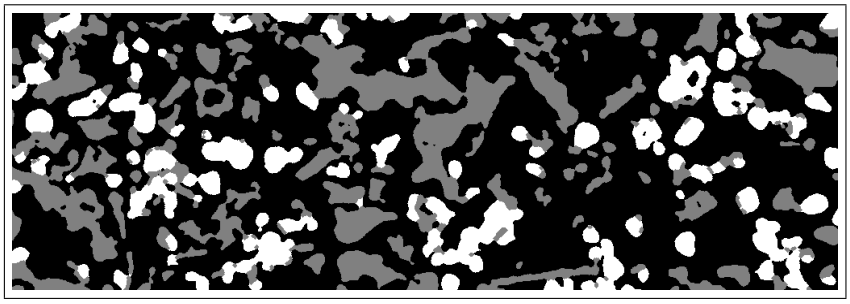

Segmented SEM image

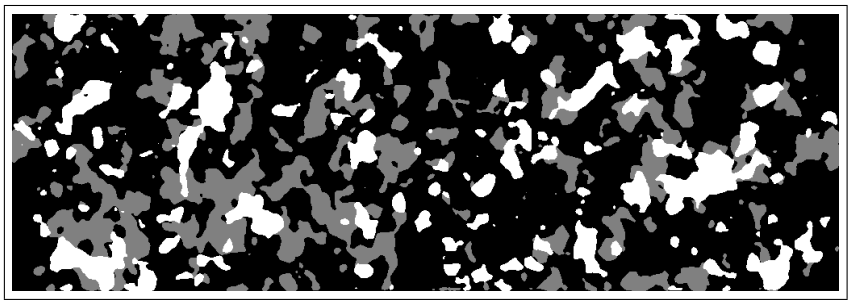

Simulated image

Figure 13: SOFC Anode. Segmented image: pores (black, $P = 0.615$), LST strontium titanate (gray, $P = 0197$), GDC Ceria (white, $P = 0.188$). Simulation by superposition of two-components thresholded Gaussian random functions [1]

When $\rho'(0) \neq 0$, we have $C'(h) = -\infty$ and the specific surface area of A_λ is infinite. Therefore, we consider the case where $\rho'(0) = 0$ and $\rho''(0) \neq 0$. From a second order Taylor expansion,

$$\rho^2(0) - \rho^2(h) = -\frac{h^2}{2} \left(\frac{\partial^2}{\partial h^2} \rho^2(h) \right)_{h=0}$$

We have

$$\begin{aligned}\frac{\partial}{\partial h}\rho^2(h) &= 2\rho(h)\rho'(h)\\ \frac{\partial^2}{\partial h^2}\rho^2(h) &= 2\rho(h)\rho''(h)+2(\rho'(h))^2\end{aligned}$$

and therefore

$$\rho^2(0)-\rho^2(h) = -h^2\rho''(0)$$

and

$$S_V = -4C'(0) = -\frac{2}{\pi}\exp(-\frac{\lambda^2}{2})\lim_{h\to 0}\frac{\rho'(h)}{h\sqrt{-\rho''(0)}} = \frac{2}{\pi}\exp(-\frac{\lambda^2}{2})\sqrt{-\rho''(0)}$$

It comes for L_{V123} [17]

$$\begin{aligned}L^*_{V123} &= \frac{\pi}{4}S'_{V1}S'_{V2}\\ &= \frac{1}{\pi}\exp(-\frac{\lambda_1^2+\lambda_2^2}{2})\sqrt{\rho''_1(0)\rho''_2(0)} \qquad (42)\end{aligned}$$

The effect of components volume fractions P'_1 and P'_2 is obtained through variables λ_1^2 and λ_2^2: $\exp(-\frac{\lambda_i^2}{2})$ is maximal (and equal to 1) for $\lambda_i = 0$, which corresponds to $P'_1 = P'_2 = \frac{1}{2}$ for the thresholded Gaussian random functions. Therefore, as for the superposition of Color Dead Leaves, the volume fractions maximizing L_{V123} are given by:

$$P_1 = \frac{1}{2},\ P_2 = \frac{1}{4},\ P_3 = \frac{1}{4}$$

As a particular case, we consider Gaussian correlation functions

$$\rho(h) = \exp(-\frac{h^2}{a^2})$$

with

$$\begin{aligned}\rho'(h) &= -\frac{2h}{a^2}\exp(-\frac{h^2}{a^2})\\ \rho''(h) &= \frac{4h^2}{a^4}\exp(-\frac{h^2}{a^2})-\frac{2}{a^2}\exp(-\frac{h^2}{a^2})\\ \rho''(0) &= -\frac{2}{a^2}\end{aligned}$$

In that case, equation (42) becomes

$$L^*_{V123} = \frac{1}{\pi}\exp(-\frac{\lambda_1^2+\lambda_2^2}{2})\frac{2}{a_1a_2} \qquad (43)$$

For sine cardinal correlation functions ([9], P. 187),

$$\begin{aligned}\rho(h) &= \frac{\sin(\frac{|h|}{a})}{\frac{|h|}{a}} \\ \rho(h) &\simeq 1 - \frac{|h|^2}{6a^2} \\ \rho'(h) &\simeq -\frac{|h|}{3a^2},\ \rho''(h) = -\frac{1}{3a^2}\end{aligned}$$

In that case, equation (42) becomes

$$L^*_{V123} = \frac{1}{\pi}\exp(-\frac{\lambda_1^2+\lambda_2^2}{2})\frac{1}{3a_1a_2} \tag{44}$$

Parameters a_i of the correlation functions $\rho(h)$ are some size parameters. As previously, microstructures with lower scales generate higher values for L^*_{V123}.

Multi scale versions of this model are obtained by linear combinations of Gaussian random functions $Z_i(x)$ with correlation functions $\rho_i(h)$, using coefficients μ_i with $\sum_i \mu_i^2 = 1$:

$$Z(x) = \sum_i \mu_i Z_i(x)$$

with correlation function $\rho(h)$:

$$\begin{aligned}\rho(h) &= \sum_i \mu_i^2 \rho_i(h) \\ \rho''(0) &= \sum_i \mu_i^2 \rho_i''(0)\end{aligned}$$

This new value of $\rho''(0)$ is then introduced in equation (42) to estimate L^*_{V123}.

6.8 Superposition of random sets defined by two thresholds of independent Gaussian RF

Consider the two random sets A_1 and A_2 defined by

$$\begin{aligned}A_1 &= \{x,\ \lambda_{11} \leq Z_1(x) < \lambda_{12}\} \\ A_2 &= \{x,\ \lambda_{21} \leq Z_2(x) < \lambda_{22}\}\end{aligned}$$

with indicator functions

$$\begin{aligned} 1_{A_1}(x) &= 1_{Z_1(x)<\lambda_{12}} - 1_{Z_1(x)<\lambda_{11}} \\ 1_{A2}(x) &= 1_{Z_2(x)<\lambda_{22}} - 1_{Z_2(x)<\lambda_{21}} \end{aligned}$$

admitting the following expansions with Hermite polynomials $H_n(z)$ ([8], p. 116):

$$\begin{aligned} 1_{A_1}(x) &= G(\lambda_{12}) - G(\lambda_{11}) + \sum_{n=1}^{\infty} \frac{H_{n-1}(\lambda_{12})g(\lambda_{12}) - H_{n-1}(\lambda_{11})g(\lambda_{11})}{n!} H_n(Z_1(x)) \\ 1_{A_2}(x) &= G(\lambda_{22}) - G(\lambda_{21}) + \sum_{n=1}^{\infty} \frac{H_{n-1}(\lambda_{22})g(\lambda_{22}) - H_{n-1}(\lambda_{21})g(\lambda_{21})}{n!} H_n(Z_2(x)) \end{aligned}$$

where G is the cumulative Gaussian distribution function. The volume fractions P_i are given by:

$$\begin{aligned} P_1 &= E\left\{1_{A_1}(x)\right\} = G(\lambda_{12}) - G(\lambda_{11}) \\ P_2 &= E\left\{1_{A2}(x)\right\} = G(\lambda_{22}) - G(\lambda_{21}) \end{aligned}$$

The centered Covariance $\overline{C}_1(h)$ is given by

$$\overline{C}_1(h) = \sum_{k=1}^{\infty} \frac{\rho_1^k}{k!} \left(H_{k-1}(\lambda_{12})g(\lambda_{12}) - H_{k-1}(\lambda_{11})g(\lambda_{11})\right)^2$$

$$\begin{aligned} \frac{\partial}{\partial \rho_1}\overline{C}_1(h) &= \sum_{k=1}^{\infty} \frac{\rho_1^{k-1}}{(k-1)!} \left(H_{k-1}(\lambda_{12})g(\lambda_{12}) - H_{k-1}(\lambda_{11})g(\lambda_{11})\right)^2 \\ &= \sum_{k=0}^{\infty} \frac{\rho_1^k}{k!} \left(H_k(z_{12})g(\lambda_{12}) - H_k(\lambda_{11})g(\lambda_{11})\right)^2 \\ &= g(\lambda_{12},\lambda_{12}) + g(\lambda_{11},\lambda_{11}) - 2g(\lambda_{11},\lambda_{12}) \end{aligned}$$

after integration with respect to ρ

$$\begin{aligned} \overline{C}_1(h) &= \frac{1}{2\pi}\int_0^{\rho_1} \left(\exp(-\frac{\lambda_{12}^2}{1+r}) + \exp(-\frac{\lambda_{11}^2}{1+r}\right) \frac{dr}{\sqrt{1-r^2}} \\ &\quad -\frac{1}{\pi}\int_0^{\rho_1} \exp\left(-\frac{1}{2(1-r^2)}(\lambda_{11}-\lambda_{12})^2\right) \exp\left(-\frac{\lambda_{11}\lambda_{12}}{1+r}\right) \frac{dr}{\sqrt{1-r^2}} \end{aligned}$$

the last term being the cross-covariance between the sets with indicator functions $1_{Z_1(x)\geq\lambda_{12}}$ and $-1_{Z_1(x)<\lambda_{11}}$.

To insure a finite specific surface area S_{V1}, we have to assume that $\rho_1'(0) = 0$ and that $\rho_1''(0) < 0$. Therefore,

$$\overline{C}_1'(0) = \frac{1}{2\pi}\sqrt{\rho_1''(0)-}\left(\exp(-\frac{\lambda_{12}^2}{2}) + \exp(-\frac{\lambda_{11}^2}{2}\right) - 2\lim_{h\to 0} g(\lambda_{11},\lambda_{12})\rho_1'(h)$$

$$\begin{aligned} g(\lambda_{11},\lambda_{12})\rho_1'(h) &= \frac{1}{2\pi\sqrt{1-\rho^2}}\exp\left(-\frac{1}{2(1-\rho^2)}(\lambda_{11}-\lambda_{12})^2\right)\exp\left(-\frac{\lambda_{11}\lambda_{12}}{1+\rho}\right) \\ &\quad \lim_{h\to 0} g(\lambda_{11},\lambda_{12})\rho_1'(h) \\ &= \frac{1}{2\pi}\sqrt{\rho_1''(0)-}\exp\left(-\frac{\lambda_{11}\lambda_{12}}{2}\right)\lim_{\rho\to 1}\exp\left(-\frac{1}{2(1-\rho^2)}(\lambda_{11}-\lambda_{12})^2\right) \\ &= 0 \end{aligned}$$

so that the specific area of contact between A_1 and the sets with indicator functions $1_{Z_1(x)\geq\lambda_{12}}$ and $-1_{Z_1(x)<\lambda_{11}}$is equal to zero, as expected, since they are separated by the set A_1. We provided a detailed calculation of the covariance $\overline{C}_1(h)$ for potential use to validate the model from image analysis measurements.

$$S_{V1} = \frac{2}{\pi}\sqrt{\rho_1''(0)-}\left(\exp(-\frac{\lambda_{12}^2}{2}) + \exp(-\frac{\lambda_{11}^2}{2}\right)$$

and finally

$$\begin{aligned} & L_{V123}^* \qquad (45) \\ = \ & \frac{1}{\pi}\left(\exp(-\frac{\lambda_{12}^2}{2}) + \exp(-\frac{\lambda_{11}^2}{2}\right)\left(\exp(-\frac{\lambda_{22}^2}{2}) + \exp(-\frac{\lambda_{21}^2}{2}\right)\sqrt{\rho_1''(0)\rho_2''(0)} \end{aligned}$$

When $\lambda_{12} \to -\infty$ and $\lambda_{22} \to -\infty$, the previous result given by equation (42) is recovered, with the same geometry. For $\lambda_{11} = \lambda_1$ and $\lambda_{21} = \lambda_2$ we obtain a microstructure where the sets A_1 has a lower volume fraction but the length L_{123}^* is higher. The model of truncated Gaussian RF with two thresholds gives access to higher specific lengths of TPB lines, as compared to the previous case with a single threshold. For instance, consider the case where $\lambda_{11} = -\lambda_{12} = \lambda_1 > 0$ and $\lambda_{22} = -\lambda_{21} = \lambda_2 > 0$. We obtain a specific triple boundary line four times higher than the result given by equation (42) for the model with a single threshold.

The condition

$$-\lambda_1 \leq Z_1(x) < \lambda_1$$

can be expressed as

$$(Z_1(x))^2 < \lambda_1$$

and the set A_1 is obtained from a single threshold of a $\chi^2(1)$ random function with 1 degree of freedom.

In these conditions, we have:

$$\begin{aligned} G(-z_1) &= 1 - G(z_1) < 1/2 \\ G(-z_2) &= 1 - G(z_2) < 1/2 \end{aligned}$$

and the volume fractions of the three components A_1, A_2, and A_3 become:

$$\begin{aligned} P_1 &= G(z_1) - G(-z_1) = 1 - 2G(-z_1) \\ P_2' &= 1 - 2G(-z_2) \\ P_2 &= 2G(-z_1)\,(1 - 2G(-z_2)) \\ P_3 &= 1 - P_1 - P_2 = 2G(-z_1) - 2G(-z_1)\,(1 - 2G(-z_2)) = 4G(-z_1)G(-z_2) \end{aligned}$$

In the case of two thresholds, P_1 is lower ($1-2G(-z_1)$ instead of $1-G(-z_1)$) and P_3 four times higher. Concerning P_2,

$$\begin{aligned} & 2G(-z_1)\,(1 - 2G(-z_2)) - G(-z_1)\,(1 - G(-z_2)) \\ = \; & G(-z_1)\,(2 - 4G(-z_2) - 1 + G(-z_2)) \\ = \; & G(-z_1)\,(1 - 3G(-z_2)) \end{aligned}$$

so that P_2 in the case of two thresholds is higher than in the case of a single threshold when $G(-z_2) < 1/3$.

More general multi-component random sets can be generated by combinations of two independent Gaussian Random Functions $Z_1(x)$ and $Z_2(x)$, using a partition of the plane (z_1, z_2) in m domains D_1, D_2,...., D_m. They provide different distribution of contacts than what is obtained for the combination of two thresholded Gaussian RF, as studied in [9] and applied in [15]. However in a simulation study, a low impact of this distribution was observed on L^*_{V123} in the case of an equirepartition of components ($P_i = \frac{1}{3}$) [15].

Covariances and order 3 moments corresponding to such partitions can be formally computed by some integrations of the bivariate and trivariate Gaussian distributions over the corresponding domains D_i [9]. They strongly depend on the partition of the plane (z_1, z_2), which has to be specified, cases studied in subsections 6.7 and 6.8 being particular examples. Concerning the consequences for $L_{V_{ijk}}$, we leave this topic involving other partitions of the plane (z_1, z_2) for further studies.

7 Discussion

We will now shortly compare our theoretical results on the length of TPB lines $L_{V_{ijk}}$ for the studied models of various random media. Then, their

predictive ability is discussed by comparison of predicted $L_{V_{ijk}}$ to some 3D measurements provided in the literature. Finally, it is interesting to discuss on the contribution of 3D information to TPB.

7.1 Potential Texture Optimization with respect to TPB lines

Our results concerning the estimation of the length of TPB lines for various models of random media illustrate the fact that a large range of values of $L_{V_{ijk}}$ can be reached, depending on the type of microstructures, even when using the same ingredients like the type of primary grain. We have to point out that in our approach the gains are not assumed to be convex, as opposite to the model proposed in [4] and [22]. For instance, for an equal volume fraction of the three components ($\frac{1}{3}$) and using the same primary grains in the construction of the model, $L_{V_{ijk}}$ is increasing when moving from an "extended microstructure model" [4], [22] (equation (4)), a mosaic model, a superposition of Boolean models, a Color Dead Leaves model (about 2 times better than the Boolean models and 7 times higher than the mosaic model). Using excursion sets of Dilution random functions, much higher length are obtained: for $m = 2$ and for $m = 5$ respectively 2 times and 6 times more than for the Boolean model model. Level sets A_n of the Dilution random function obtained by setting $N(x) = n$ generate textures with much higher TPB lines lengths with comparison to the Boolean model: 5 times for $n = 1$, 10 times for $n = 2$, 14 times for $n = 3$, and 20 times for $n = 4$. This wide range of $L_{V_{ijk}}$ values is a consequence of the increasing degree of fragmentation of the texture, depending on the model, and reveals the potential of our approach to the design of new materials with improved performances.

7.2 Predictive ability of the models

In order to evaluate the ability of the models to predict experimental values of $L_{V_{ijk}}$, we consider some results on Ni-YSZ electrodes ([15], cathode in [18] and anode in [19]). In these publications, 3D micrographs of electrodes were analyzed, providing the following measured information: P_i, d_i (average component diameter), S_{V_i}, and $L_{V_{ijk}}$. Having no way to fit a morphological model on these microstructure, we made the following simplified assumption: each component of the microstructure Ni and YSZ is made of a Boolean model of spheres with diameter equal to d_i, so that

$$\frac{\overline{S}(A_i')}{\overline{V}(A_i')} = \frac{6}{d_i}$$

	[19]	CFL [18]	Cathode [18]	Cell A [15]	Cell B [15]
P_{YSZ}	0.33	0.49	0.317	0.44	0.4955
d_{YSZ}	$0.55\mu m$	$0.73\mu m$	$1.1\mu m$	$0.6\mu m$	$0.6\mu m$
S_{VYSZ}	$4.24\mu m^{-1}$	$5.5\mu m^{-1}$	$6.01\mu m^{-1}$	$3.68\mu m^{-1}$	$3.42\mu m^{-1}$
P_{Ni}	0.26	0.282	0.217	0.28	0.24
d_{Ni}	$0.9\mu m$	$0.83\mu m$	$1.2\mu m$	$1\mu m$	$0.8\mu m$
S_{VNi}	$2.33\mu m^{-1}$	$6.54\mu m^{-1}$	$5.87\mu m^{-1}$	$2.30\mu m^{-1}$	$2.46\mu m^{-1}$
$L_{V_{ijk}}$	$11.2\mu m^{-2}$	$4.63\mu m^{-2}$	$3.46\mu m^{-2}$	*active:* $4.78\mu m^{-2}$	*active:* $6.2\mu m^{-2}$
$L^*_{V_{ijk}1}$	$4.5\mu m^{-2}$	$4.05\mu m^{-2}$	$1.27\mu m^{-2}$	$1.68\mu m^{-2}$	$4.5\mu m^{-2}$
$L^*_{V_{ijk}2}$	$4.63\mu m^{-2}$	$5.75\mu m^{-2}$	$1.45\mu m^{-2}$	$5.55\mu m^{-2}$	$6.93\mu m^{-2}$

Table 2: Comparison between experimental and theoretical lengths of TPB lines in Ni-YSZ electrodes

The random microstructure for comparison is then obtained by the superposition of the two Boolean models. Therefore two constructions are available, with A_1 representing either Ni or YSZ (providing the estimates $L^*_{V_{ijk}1}$ and $L^*_{V_{ijk}2}$). These assumptions are rather crude: grains are not spherical and the way to measure d_i differ according to papers; since in [15] d_i obtained from a 3D size distribution made by morphological openings provide very low values as a result of a lot of small details in the microstructure, we replaced them by the range of covariances (or correlation length) which is approximately deduced from figures 6 (a,b) in [15]. With these simplifications, we can provide rough estimates of $L_{V_{ijk}}$ to be compared to experimental data. Data and predictions are collected in table 2. For three cases (column 2, 4, 5), there is a good agreement between predicted and measured $L_{V_{ijk}}$. Concerning Cell A and Cell B, the total length is of course longer than the active length restricted to the measurement for percolating lines. Moreover, the authors of [15] could fit the observed microstructure to a model based on thresholded Gaussian random functions, which differs from the combination of Boolean models. An underestimation, with a factor of the order of 2.5, is obtained for the [19] and the cathode [18] specimens. Higher predicted values could be obtained, using other models like the Color Dead Leaves model. Therefore, the rough estimations of $L_{V_{ijk}}$ deduced from a somewhat arbitrary model, and without fitting its parameters to data, are correct in 3 cases out of 5 taken from 3 publications. This result validates our theoretical approach. Furthermore, since the model used for the validation of our results does not show the best performances concerning $L_{V_{ijk}}$, a large improvement of $L_{V_{ijk}}$ of real electrodes can be expected for an appropriate choice of their

microstructure.

7.3 3D versus 2D information for TPB lines

As is clearly seen in this presentation, $L_{V_{ijk}}$ can be estimated with planar observations, by counting on 2D images of the microstructure the 24 configurations of the triple $\{i, j, k\}$ and of the rotations of the set of testing points $\{x, x + h_1, x + h_2\}$, applying equation (1). Another approach is based on the implementation of models of random sets, after identification of their parameters from morphological measurements like covariances on images, as done in [1] for SOFC materials.

Alternatively, when 3D images are available, either experimentally or from 3D simulations of microstructures, triple lines can be extracted to provide a direct estimation of $L_{V_{ijk}}$. This approach is rather costly, and requires to get statistically representative data. The main advantage is that it enables us to extract percolating components and particularly active TPB lines.

Available data on 3D simulations or from 3D real microstructures reconstructions of Solid Oxide Fuel Cells show that a significant proportion of total TPB lines are active: 0.87 in [22], 0.8 in [4], 0.75 and 0.71 in [18], 0.66 in [19], 0.63 in [20], 0.5 in [21]. Therefore, the theoretical prediction of $L_{V_{ijk}}$ is useful and practical, provided that the components of the model percolate. In addition, developing random models with analytical results is very fruitful, since systematic studies of the impact of the choice of a particular model and of its parameters can be made, avoiding long and clumsy empirical approaches.

8 Conclusion

Theoretical estimates of the specific length of triple phase boundary lines $L_{V_{ijk}}$ were derived for a broad range of multi-component random structures. Since analytical results are obtained, it is easy to look for so-called optimal microstructures with respect to this parameter. A noticeable point is that the effects of the composition, through volume fractions, and of the morphology, through the choice of primary grains, are separate, so that any "optimal composition" is derived independently on the geometry.

Since $L_{V_{ijk}}$ is inversely proportional to the square of a length scale of the microstructure, it shows a quadratic growth with the inverse of this length scale, so that fine microstructures allow to increase $L_{V_{ijk}}$. The impact of the length scale on $L_{V_{ijk}}$ is much more effective than the impact of the composition through volume fractions.

Our theoretical approach was validated by comparison of the predicted $L_{V_{ijk}}$ to some measurements made on 3D images of materials.

Models designed with the same basic primary grains may show a large range of values for $L_{V_{ijk}}$, depending on their mode of construction. Much longer $L_{V_{ijk}}$ than what is observed in real materials from 3D observations can be obtained. This opens up promising avenues for improving the electrochemical behavior of fuel cell components.

References

[1] Abdallah B., Willot F., Jeulin D. (2016) Morphological modelling of three-phase microstructures of anode layers using SEM images, Journal of microscopy, 2016, vol. 263, no 1, p. 51-63.

[2] Chiu S. N., Stoyan D., Kendall W. S., & Mecke J. (2013). Stochastic geometry and its applications, John Wiley & Sons.

[3] Gilbert E.N. (1962) Random subdivisions of space into crystals, Ann. Math. Stat., Vol. 33, pp. 958-972.

[4] Gokhale, A. M., Zhang, S., & Liu, M. (2009). A stochastic geometry based model for total triple phase boundary length in composite cathodes for solid oxide fuel cells. Journal of Power Sources, 194(1), 303-312.

[5] Greco A., Jeulin D., Serra J. (1979) The use of the texture analyser to study sinter structure: application to the morphology of calcium ferrites encountered in basic sinters of rich iron ores, Journal of Microscopy, 116, pp. 199-211.

[6] Jeulin D. (1979) Morphologie Mathématique et Propriétés Physiques des agglomérés de minerais de fer et du coke métallurgique, Thèse de Docteur-Ingénieur en Sciences et Techniques Minières, Option Géostatistique, Ecole des Mines de Paris, 23 Novembre 1979 (298p.).

[7] Jeulin D. (1980) Multi-component random models for the description of complex microstructures, Proc. 5th International Congress for Stereology, Mikroskopie, Vol. 37 S: 130-137.

[8] Jeulin D. (2021) Morphological models of random structures, Springer Verlag.

[9] Lantuéjoul Ch. (2002) Geostatistical Simulation, Models and Algorithms, Springer.

[10] Lanzini A., Leone P., Asinari P. (2009) Microstructural characterization of solid oxide fuel cell electrodes by image analysis technique, Journal of Power Sources, 2009, vol. 194, no 1, p. 408-422.

[11] Masson D., Abdallah B., Willot F., Jeulin D., Mercadelli E., Sanson A., Chesnaud A., Thorel A. (2015) Morphological modelling of a metal foam supported SOFC configuration. ECS Transactions, 68(1), 2951.

[12] Matheron G. (1968) Schéma booléen séquentiel de partition aléatoire, N-83 CMM, Paris School of Mines publication.

[13] Matheron G. (1975) Random sets and Integral Geometry, Wiley.

[14] Miles R. E. (1972) Multi-dimensional perspectives on stereology. Journal of Microscopy, 95(2), 181-195.

[15] Moussaoui H., Laurencin J., Gavet Y., Delette G., Hubert M., Cloetens P., Le Bihan T., Debayle J. (2018) Stochastic geometrical modeling of solid oxide cells electrodes validated on 3D reconstructions. Computational Materials Science, 143, 262-276.

[16] Nagel, W., & Weiss, V. (2005). Crack STIT tessellations: characterization of stationary random tessellations stable with respect to iteration. Advances in applied probability, 37(4), 859-883.

[17] Neumann M., Abdallah B., Holzer L., Willot F., Schmidt V. (2019) Stochastic 3D modeling of three-phase microstructures for predicting transport properties: a case study. Transport in Porous Media, 128(1), 179-200.

[18] Usseglio-Viretta F., Laurencin J., Delette G., Villanova J., Cloetens P., Leguillon D. (2014) Quantitative microstructure characterization of a Ni–YSZ bi-layer coupled with simulated electrode polarisation. Journal of Power Sources, 256, 394-403.

[19] Vivet N., Chupin S., Estrade E., Piquero T., Pommier P. L., Rochais D., Bruneton E. (2011) 3D Microstructural characterization of a solid oxide fuel cell anode reconstructed by focused ion beam tomography. Journal of Power Sources, 196(18), 7541-7549.

[20] Wilson J. R., Kobsiriphat W., Mendoza R., Chen H. Y., Hiller J. M., Miller D. J., Thornton K., Voorhees P. W., Adler S. B., Barnett S. A. (2006) Three-dimensional reconstruction of a solid-oxide fuel-cell anode. Nature materials, 5(7), 541-544.

[21] Wilson J. R., Cronin J. S., Duong A. T., Rukes S., Chen, H. Y. Thornton K., Mumm D.R., Barnett S. (2010). Effect of composition of (La0. 8Sr0. 2MnO3–Y2O3-stabilized ZrO2) cathodes: Correlating three-dimensional microstructure and polarization resistance. Journal of Power Sources, 195(7), 1829-1840.

[22] Zhang, S., & Gokhale, A. M. (2012). Computer simulations of topological connectivity of the triple phase boundaries in solid oxide fuel cell composite cathodes. Journal of Power Sources, 219, 172-179.

[23] Zhu W., Ding D., Xia C. (2008) Enhancement in three-phase boundary of SOFC electrodes by an ion impregnation method: a modeling comparison. Electrochemical and solid-state letters, 11(6), B83.